Review

Zdzisław Jaworski*, Tadeusz Spychaj, Anna Story and Grzegorz Story

Carbomer microgels as model yield-stress fluids

https://doi.org/10.1515/revce-2020-0016
Received February 24, 2020; accepted March 3, 2021;
published online April 27, 2021

Abstract: The review presents current research results for Carbopol-based microgels as yield-stress materials, covering three aspects: chemical, physical and rheological. Such a joint three-aspect study has no analog in the literature. The chemical aspects of Carbopol polymers are presented in terms of a cross-linking polymerization of acrylic acid, their molecular structure, microgel formulation, polyacid dissociation and neutralization, osmotic pressure and associated immense microgel swelling. The physical characterization is focused on models of the shear-induced solid-to-liquid transition of microgels, which are formed of mesoscopic particles typical for soft matter materials. Models that describe interparticle effects are presented to explain the energy states of microgel particles at the mesoscale of scrutiny. Typical representatives of the models utilize attributes of jamming dispersions, micromechanical and polyelectrolyte reactions. Selected relationships that result from the models, such as scaling rules and nondimensional flow characteristics are also presented. The rheological part presents the discussion of problems of yield stress in 2D and 3D deformations, appearance and magnitude of the wall slip. The theory and characteristics of Carbopol microgel deformation in rotational rheometers are presented with graphs for the steady-state measurements, stress-controlled oscillation and two types of transient shear deformation. The review is concluded with suggestions for future research.

Keywords: Carbopol; characterization; chemical; hydrogel; physical; rheological.

***Corresponding author: Zdzisław Jaworski,** Faculty of Chemical Technology and Engineering, West Pomeranian University of Technology, Aleja Piastow 42, 71-065, Szczecin, Poland, E-mail: Zdzislaw.Jaworski@zut.edu.pl
Tadeusz Spychaj, Anna Story and Grzegorz Story, Faculty of Chemical Technology and Engineering, West Pomeranian University of Technology, Aleja Piastow 42, 71-065, Szczecin, Poland, E-mail: Tadeusz.Spychaj@zut.edu.pl (T. Spychaj), Anna.Story@zut.edu.pl (A. Story), Grzegorz.Story@zut.edu.pl (G. Story)

1 Introduction

Introduction of the "yield stress" term can be related to the characterization in the British Standard 5168 dated 1875, which reads: "that stress below which the substance is an elastic solid and above it a liquid" (cited after (Barnes and Walters 1985)). Such yield-stress fluids (YSFs) are abundant in the environment and can be found both in living organisms and used in many industrial processes (Ahmed 2015; Aufderhorst-Roberts et al. 2018; Balmforth et al. 2014; Lefrancois et al. 2015). The fluids constitute the main body of soft condensed matter but different material types are ranked among the yield-stress fluids (Bonn et al. 2017; Joshi and Petekidis 2018), e.g., granular suspensions, colloidal pastes, concentrated emulsions or foams. For more than a century, we have been deepening our understanding of the solid-to-liquid and liquid-to-solid transformation of the YSF. The initial research advances can be attributed to rheologists who were then supported by physicists and polymer chemists (Coussot 2017). Perhaps one of the central scientific problems in YSFs of the last three decades was to convincingly decide whether the yield stress is reality or a myth as implied by Barnes and Walters (1985). Beneficially, significant progress in the physical theory and experiments was made in the last 20 years (Coussot 2017; Malkin et al. 2017).

Various similar but not equivalent names of yield-stress fluids have been used in the subject literature throughout the last 80 years. Rheologists characterized the materials either as viscoplastic, equivalent to Herschel-Bulkley fluids (Bonn et al. 2017; Putz and Burghelea 2009), elasto-viscoplastic (Dimitriou et al. 2013) or thixotropic viscoplastic (Mendes 2009). By contrast, physicists used to describe the materials as forms of soft matter: systems composed of soft solid particles, soft glassy materials, soft colloids/jammed systems, soft matter/materials as well as soft particle suspensions/pastes/glasses. On the other hand, chemical engineers and polymer chemists preferred using the following descriptions of YSFs: microgels, polymer/colloidal gels/dispersions, polyelectrolyte/macroion

gels, microgel/latex/carbomer dispersions/suspensions, or hydrogels. Such a rich variety of labels for Carbopol dispersions calls for using lesser names and perhaps the two historically first descriptions: "yield-stress fluids" or "microgels" are interchangeably used throughout the present study for Carbopol dispersions only. Rodriguez et al. (1994) defined microgels as "aqueous dispersions of internally cross-linked, acid-containing lattices." That definition has been used in many other papers and also in this review though it differs from the original one for nonelectrolyte organic macromolecules (Baker 1949).

1.1 Yield stress: introduction

It is therefore informative to recall the definitions of yield stress recommended by the Compendium of Chemical Terminology of IUPAC in 1997 and confront them with recent views (IUPAC 1997). Yield stress was then regarded as "the shear stress at which yielding starts abruptly" and "its value depends on the criterion used to determine when yielding occurs" (IUPAC 1997). A decreasing, finite shear stress when such soft materials stop flowing and start behaving as a solid is the yield stress, τ_y, defined in the limit when the deformation rate, $\dot{\gamma}$, goes to zero (Ikeda et al. 2012; Malkin et al. 2017).

$$\tau_y = \lim_{\dot{\gamma}\to 0} \tau\,(\dot{\gamma}) \tag{1-1}$$

That extrapolation is referred to as the dynamic yield stress (Bonn et al. 2017). A variety of measurement techniques have been used in determination of the yield stress and they include: steady-state flow curve, the maximum of stress overshoot in start-up flows, stress relaxation, oscillatory mode, creep and recovery (Dinkgreve et al. 2016; Mewis and Wagner 2012).

Continuous progress in the physical and rheological characterization of yield-stress materials has resulted in other definitions. In particular, the following yield stress types were defined in the subject literature: static, dynamic, apparent, absolute (ideal), compressive and elastic. However, the static and dynamic versions have been the most frequently used types of yield stress. According to Fall et al. (2010) "the static yield stress would be the stress above which the material turns from a solid state to a liquid one, while the dynamic yield stress is the stress where the material turns from a liquid state to a solid one." Identical definitions were used in other studies and such definitions are now in general use (Dinkgreve et al. 2016; Joshi and Petekidis 2018). It was also suggested the yield stress is the limit between the aging stresses and rejuvenating stresses exerted on the material (Moller et al. 2009a). Above the stress threshold the material undergoes complex delayed yielding before a homogeneous steady state is reached Divoux et al. (2011a). A simple yield-stress material flows with time-independent viscosity but below that limit the steady-state apparent viscosity grows infinitely (Moller et al. 2009a).

In rheology, several relationships of shear stress, τ, vs. shear rate$\dot{\gamma}$, were proposed for the yield-stress fluids and the most popular is the Herschel-Bulkley (H-B) model (Herschel and Bulkley 1926):

$$\tau = \tau_y + k\dot{\gamma}^n \tag{1-2}$$

with two model constants, k and n. The parameters of the original model were named material constants (Herschel and Bulkley 1926). The exponent, n, is called the exponent of power-law part of the H-B model (Barnes 1999) or power-law index (Shafiei et al. 2017) and its value for different Carbopol microgels of concentration above 0.1% wt. was found in the range from 0.3 to 0.7 (Divoux et al. 2011a), Table 1. The k constant (consistency index) is the coefficient of the power-law part of Eq. (1-2) and its value for such Carbopol microgels ranges widely from 0.4 to 100 and is usually smaller for larger n exponent. More information is provided in Table 1 and the reasons for such wide spreads of the model parameters remain unresolved in the literature.

The viscous part of the model represents the contribution from shearing,

$$\mu = k\dot{\gamma}^{n-1} \tag{1-3}$$

to the effective (apparent) viscosity, μ_{app}:

$$\mu_{\text{app}} = k\dot{\gamma}^{n-1} + \frac{\tau_y}{\dot{\gamma}} \tag{1-4}$$

Advanced information on yield stress can be found in Section 4 on rheological characterization of Carbopol microgels.

Several research tools were engaged in the investigations of YSFs. In addition to a broad range of macroscopic rheological measurements, physical experimental and modeling tools were successfully applied to investigate mesoscopic properties at micrometer scale. Since the two characteristics depend on molecular scale interactions, important contributions resulted also from chemical studies of YSFs. However, in the most advanced studies two or all three described methods of analysis were involved (Bonn et al. 2017; Cloitre et al. 2003b; Coussot et al. 2017; Divoux et al. 2012; Piau 2007; Tan et al. 2010; Tan et al. 2004).

Table 1: Published parameters of Herschel-Bulkley relationship.

Carbopol type	Weight concentration (%)	pH	τ_y (Pa)	k (Pa s^n)	n (–)	G_0 (Pa)	References
901	0.5	–	43	23	0.43	200	Dimitriou and McKinley (2019)
934	0.5	6–7	44	52.8	0.3	–	(Piau 2007) interpreted (Uhlherr et al. 2005)
934	1.0–3.0	4.0–12.1	58.1–359	17.5–118.2	0.31–0.39	550–1002	Shafiei et al. (2017)
940	0.17	4.6	18.9	4.58	0.46	–	Hirata et al. (1994)
940	0.17	4.6	18.9	4.6	0.46		Moore et al. (1995)
940	1.48	2.8–11.5	30.3–167	3.37–27.8	0.5	–	Curran et al. (2000)
940	0.1	4.6	1.3–2.6	0.37–0.54	0.55–0.58	–	Adams and Barigou (2007)
940	0.26	7.3	46	39.6	0.37	–	Piau (2007)
940	1.0	7.0	84	72.2	0.37	–	(Piau 2007) fitted (Magnin and Piau 1990)
940	0.3	7.0	~20	–	–	250	Benmouffok-Benbelkacem et al. (2010)
940	0.1–0.2	6.2–7.0	10.5–91	2.67–46.8	0.24–0.48	–	Gomez et al. (2010)
940	0.2	~7	19–21	5.75	0.42	337	Aktas et al. (2014)
940	0.1	4.5	3.2	0.26	0.7	–	Alberini et al. (2014)
	0.2	5.0	25.2	6.74	0.42		
940	0.12	7.1	19.2	5.4	0.38	~120	Ortega-Avila et al. (2016)
940	1.0	7.3	131	39	0.32	620	Ahonguio et al. (2016b)
940	1.0	7.3	125	30	0.33	625	Ahonguio et al. (2016a)
940	0.14	6.0	10.5	4.4	0.38	–	Liu et al. (2018)
940	2.0; 3.0	2.1–12.4	61.7–348.6	2.2.–41.5	0.43–0.82	~320–900	Shafiei et al. (2018)
940	0.2	7.0	20	–	–	–	Agarwal and Joshi (2019)
941	0.33–6.16	7.0	60–600	–	0.37	125–1320	Ketz et al. (1988)
980 new 940	0.06–0.20	7.0	0.41–37.0	0.005–19.3	0.35–0.95	–	Kelessidis and Hatzistamou (2011)
980	0.045–1.0	7.0	0.03–115	0.12–100	0.30–0.60	–	Roberts and Barnes (2001)
980	0.1–0.2	7.0	~24–80	1–26	0.28–0.60	100–8000	Weber et al. (2012)
980	0.12–0.20	6.1–6.5	9.3–42.8	2.4–11.8	0.41–0.48	–	Russell et al. (2019)
980 NF	0.10–0.15	Neutral	2.71–10.9	1.32–5.46	0.38–0.48	~10–40	Varges et al. (2019)
981	0.1–0.5	7.0	1.16–13.0	1.58–15.1	0.42–0.47	–	Jofore et al. (2015)
ETD2020	0.05–0.2	~6	2.6–12.2	–	–	–	Bhattacharjee et al. (2018)
ETD2050 (like941)	0.1–1.0	3.4–11.0	1.74–33.8	2.76–34.1	0.33–0.55	20–215	Di Giuseppe et al. (2015)
ETD2050	0.5; 1.2	6.0	5.8; 13.9	5.0; 9.8	0.5	–	Toplak et al. (2007)
ETD2050	0.8	–	0.35	1.57	0.5	–	Davaille et al. (2013)
ETD2050	0.25–1.0	~7	1.15–13.7	1.39–5.79	0.53–0.56	–	Geraud et al. (2013)
ETD2050	1.0	7.0	10.2	3.3	0.60	37	Lidon et al. (2017)
ETD2623	0.1–1.0	5.5–5.7	0.83–10.6	9.26–102	0.30–0.50	125–610	Di Giuseppe et al. (2015)
EZ2 (like 980)	0.1125–0.14	~4.8	1.17–3.12	4.49–20.44	0.26–0.60	–	Taghavi et al. (2012)
EZ2	0.5–1.0	6.8–7.1	82–138	21.7–32.0	0.42–0.44	654–1020	Di Giuseppe et al. (2015)
EZ3	0.5–1.0	7.0–7.4	153–258	50.1–80.8	0.383–0.385	675–1000	Di Giuseppe et al. (2015)
Ultrez 10	1.5	7	105.8	48.3	0.416	–	Rabideau et al. (2009)
Ultrez 10	0.15, 0.20	7.0	8.1–20.1	9.02–16.6	0.42–0.43	–	Kelessidis and Hatzistamou (2011)
Ultrez 10	0.1–0.5	7.0	~3–23	–	~0.38–0.57	~20–330	Gutowski et al. (2012)
Ultrez 10	0.1–5.0	2.5–7.0	0.81–139	3.16–40.8	0.29–0.57	66–1090	Di Giuseppe et al. (2015)
Ultrez 10	0.7		66.5	28.1	0.4	384	de Cagny et al. (2019)
Ultrez 20	0.02–0.2	7.0	0.0015–32.5	0.0015–21.5	0.30–0.99	~160	Hassan et al. (2015)
Ultrez 21	0.1–1.0	6.5–7.0	0.36–224	1.39–23.8	0.41–0.64	31–750	Di Giuseppe et al. (2015)

1.2 Carbopol: preliminary remarks

Water-swellable microgels have been offered commercially since the 1950s (Carnali and Naser 1992). One of commonly used types of yield-stress fluids are carbomers, also named Carbopol. Till now, a range of carbomer variants has been commercially available. Their current practical applications are mainly in various oral pharmaceuticals and cosmetics and also in topical lotions, gels and creams (Lubrizol 2018a). The function of carbomers in aqueous formulations is to build viscosity, form gels, stabilize emulsions, and suspend particles. Carbopol hydrogels have been widely used also in research as model translucent YSFs (Benmouffok-Benbelkacem et al. 2010; Cloitre and Bonnecaze 2017; Curran et al. 2002; Ovarlez et al. 2013), being very convenient in anemometric and light scattering measurements. Perhaps the first authors who published in 1961 systematic rheological investigations of Carbopol dispersions were Fischer et al. (1961). They measured yield stress for varied pH, concentration and temperature and confirmed Carbopol dispersions obeyed the Herschel-Bulkley relationship. Such microgels have been used as model systems in fundamental research (Balmforth et al. 2014). Carbopol 940 was the most common type used in research being considered as the standard for industry and probably the least expensive though not low-cost in absolute terms (Kelessidis and Hatzistamou 2011). In another systematic rheological study, data of Carbopol hydrogels were applied in the modeling of geological processes (Di Giuseppe et al. 2015). Importantly, Moller et al. (2009b) and review papers on YSF properties (Bonn et al. 2017; Ovarlez et al. 2013) presented Carbopol microgels as nonthixotropic simple yield-stress fluids. Many other authors consider Carbopol microgels as nonthixotropic (simple) yield-stress material (Bonn et al. 2017; Coussot et al. 2009; Curran et al. 2002; Hassan et al. 2015; Moller et al. 2009a; Ortega-Avila et al. 2016; Ovarlez et al. 2013; Piau 2007). However, a small extent of thixotropic behavior of a few Carbopol dispersions was found by others (Blackwell and Ewoldt 2016; Dinkgreve et al. 2018a; Islam et al. 2004). It can also be supposed that a fraction of small (below 1 μm) microgel particles plays the key role in demonstration of that minor thixotropy, which was observed for long and strongly stirred microgels of Carbopol Ultrez 10 (Dinkgreve et al. 2018a).

Due to their favorable properties, carbomer hydrogels were chosen for detailed description in this paper, elucidating results of three types of current insight – chemical, physical and rheological. Although those methods have usually applied different scales of scrutiny, they are extremely complementary. Therefore, this work is meant to serve specialists in one of the three disciplines with an overview of the main results of the two other methods. Finally, an attempt is undertaken to propose potential synergistic use of the three approaches and provide recommendations on the use of carbomers as model yield-stress fluids.

2 Chemical characterization of carbomer microgels

This Section contains information of the following chemical aspects of Carbopol: nomenclature, synthesis, new types, structure, properties, formulation, dissociation, neutralization, osmotic pressure, swelling and microgel processing.

2.1 Nomenclature

“Carbomer” is one of the generic names that can be used to describe Carbopol® polymers. Carbomer can be defined as a high molecular weight polymer of acrylic acid crosslinked with allyl ethers of polyalcohols. The United States Pharmacopeia and European Pharmacopeia include various carbomer monographs. The European Pharmacopeia has only one monograph which applies to Carbopol® polymers called “Carbomers”. Similarly, the Japanese Pharmaceutical Excipients also has a single monograph called “Carboxyvinyl Polymer”. The United States Pharmacopeia/National Formulary has several monographs for different carbomer grades. The monographs called “Carbomer XXX” (where XXX is a numerical designation) were assigned to products manufactured with benzene. Additionally, there are three umbrella monographs that separate carbomer products based on polymer structure. These three monographs are “Carbomer Copolymer” “Carbomer Homopolymer” and “Carbomer Interpolymer” and they apply to products not polymerized in benzene (Lochhead 2017).

2.2 Synthesis

Generally, covalently crosslinked acrylic acid carbomers are produced via precipitation polymerization at temperature ranging from 20 to 90 °C. The monomer is polymerized in a medium which is a solvent for the monomer but nonsolvent for the polymer. That technology is used industrially to produce Carbopol polymers (Herth et al. 2016). Acrylic acid

based hydrogels, mainly for industrial applications, can be directly synthesized (Ahmed 2015). Carbomer particles have the true density of about 1410 kg/m^3, bulk density of approx. 208 kg/m^3 (Panzade and Puranik 2010). The particles have a very expanded morphology with the BET surface area of 12–14 m^2/g (Lubrizol 2018b). In the subject literature, there are research reports on using several types of carbomers, initially with a specific "XXX" extension, such as Carbopol XXX. However, further extensions have been used by manufacturers as well. Examples of those products used in the pharmaceutical and cosmetic applications were listed by (Manzo et al. 2014; Panzade and Puranik 2010; Patel et al. 2006). Practical applications and selected characteristics of earlier Carbopol types are published on the manufacturer site (Lubrizol 2018a), although detailed information about Carbopol types was recently made inaccessible and this makes thorough comparison of Carbopol types virtually impossible.

2.3 New trademarks

Considering environmental reasons and final designation of these polymers, new environmentally acceptable solvents, such as ethyl acetate (EAc) or cosolvent mixture EAc/cyclohexane (instead of benzene), have been applied for Carbopol Ultrez-type syntheses. The family of Carbopol Ultrez (CU) products is composed of either carbomers, such as homopolymers Carbopol Ultrez 10 (CU10) and Carbopol Ultrez 30 (CU30), or acrylates/alkyl acrylate copolymers, such as Carbopol Ultrez 20 (CU20) and Carbopol Ultrez 21 (CU21). The cross-linking agents of those basic polymers are polyethers like either polyallyl pentaerythritol (e.g., tetraallyl pentaerythritol, TAPE) or polyallyl sucrose (e.g., hexaallyl sucrose) in the cases of acrylic acid homopolymers (CU10 and CU30) (Lochhead 2017), or polyallyl pentaerythritol in copolymers (CU20 and CU21) (Lubrizol 2018a). A compilation of data available in 2018 on the new types of Carbopol is presented in Tables 2 and 3 (Lubrizol 2008).

It follows from the data in Tables 2 and 3 that Carbopol easily forms water suspensions of different concentrations. Neutralized Carbopol dispersions can have very high clarity, have low toxicity and can be used as an effective thickener with yield stress values selectable in broad range. The presented Carbopol features allow to consider Carbopol microgels as model yield stress materials since their flow curves well conform to the Herschel-Bulkley model (Curran et al. 2002; Ovarlez et al. 2013). Furthermore, it was concluded that "Carbopol gels prove to be relatively simple and very useful benchmark model materials" (Piau 2007).

2.4 Chemical structure

The resultant macromolecules are formed by cross-linking of few (4 in case of TAPE) linear chains of polyacrylic acid, PAA, -[CH_2-CH(COOH)]-. Therefore, such crosslinker plays the role of a node in the polymer network, see Figure 1(b and c). The amount of a crosslinker in carbomers is generally at the level of few percent by weight, e.g., 0.5–2% (Hsu 1997) or 0.2–3.0% (Thomas et al. 2006), and usually

Table 2: General description and characteristics of Carbopol® Ultrez polymers.

No.	Feature/polymer	Carbopol® Ultrez 10	Carbopol® Ultrez 20	Carbopol® Ultrez 21	Carbopol® Ultrez 30
1	Polymer type according to INCI	Carbomer	Acrylates/C_{10-30} alkyl acrylate crosspolymer	Acrylates/C_{10-30} alkyl acrylate crosspolymer	Carbomer
2	Cross-linking agent	Polyallyl pentaerythritol	Polyallyl pentaerythritol	Polyallyl pentaerythritol	Polyallyl sucrose
3	Polymerization environment	Toxicologically-preferred cosolvent system (EAc/cyclohexane)	No data	Toxicologically- preferred cosolvent system (EAC/cyclohexane)	Toxicologically- preferred cosolvent system (EAC/cyclohexane)
4	Short rheological description	Extremely efficient rheology modifier	Rheology modifier and stabilizer	Extremely efficient rheology modifier, gives clear gels	Rheology modifier in a broad pH range
5	Suspending ability (yield value dependent)	High	High	High	Very high
6	Main application areas	Clear gels, hydroalcoholic gels, creams and lotions	Shampoos, body washes, gels lotions and creams	Clear gels, hydroalcoholic gels, creams and lotions	Formulations with botanical extracts or salts, as well as acidic ingredients

INCI, International Nomenclature for Cosmetic Ingredients; EAc, ethyl acetate.

Table 3: Closer characteristics of the representative Carbopol® Ultrez aqueous systems.

No.	Feature/polymer	Carbopol® Ultrez 10	Carbopol® Ultrez 20	Carbopol® Ultrez 21
1	Wetting characteristics	Easy to disperse in water (5 min/0.5 wt.%/25 °C)	Exceptionally easy dispersible in water (self-wets; 3 min/ 0.5 wt.%/25 °C)	Exceptionally easy dispersible in water (self-wets; 2–3 min/0.5 wt.%/25 °C)
2	Relative viscosity:			
	– Polymer suspension 3 wt.% (pH = 2.5–3.5)	– e.g. ca. 500 mPa·s	– e.g. ca. 4000 mPa·s	– e.g. ca. 1500 mPa·s
	– Polymer 0.5 wt.% after neutralization (pH = 6.0–7.5)	– e.g. ca. 51, 000 mPa·s	– e.g. ca. 26, 000 mPa·s	– e.g. ca. 56, 000 mPa·s
	– Polymer 1 wt.% after neutralization (pH = 7.5) before and after NaCl, 0.1 wt.% addition	– e.g. 79, 000 → 57, 000 mPa·s	– e.g. 48, 000 → 40, 000 mPa·s	– e.g. ca. 87, 000 → 64, 000 mPa·s
3	Yield value (and viscosity) for polymer suspension (pH = 4.0, 0.4 wt.%, 25 °C)	– e.g. 91 Pa (7700 mPas)	– e.g. 25.6 Pa (3400 mPas)	No data
4	Relative ion tolerance	Low	High	Medium
5	Relative shear tolerance	High	Low	High
6	Clarity:			
	– General	– Low	– High	– Very high
	– At polymer concentration:			
	0.1 wt.%	No data	>99%	>98.5%
	0.5 wt.%	No data	>99%	>98.5%
	1.0 wt.% (pH = 6.0/25 °C/1 h)	No data	>98%	~96%

close to 1.0% as shown in cited examples. The number of monomers between adjacent cross-links is high and was estimated at 1450–3300 (Carnali and Naser 1992; Gomez-Carracedo et al. 2004). Carbomer molecules lie at the top end of molecular masses for polymers (Lochhead 2017). A consequence of the carbomer colloidal-type state in aqueous systems is a very problematic molecular mass determination by means of available experimental techniques (Lubrizol 2007). According to Shafiei et al. (2018) the molecular weight of carbomers ranges between 3 and 4 billion of Daltons, while the producer suggests its value up to 4.5 billion (Lubrizol 2007). Another source (Lochhead 2017) suggests a smaller range of 10^8–10^9, a further source estimates the molecular weight between 3 and 20 million of Daltons, whereas others report the range of 1–4 million, depending on the degree of cross-linking (Gomez-Carracedo et al. 2004; Labanda et al. 2004; Muramatsu et al. 2000). Apart from the amount of cross-linking agents, such a wide range of molecular weight of commercial Carbopols may result from homogenization quality of the polymerization reactants and also from limited accuracy of the measurement procedure(s). Although that spread may result from a rich variety of Carbopol brands, it nevertheless corresponds to roughly million monomers of acrylic acid, CH_2=CH–COOH, in a carbomer macromolecule. A graphic representation of polymeric chains of Carbopol in the dry (coiled), and hydrated and neutralized (stretched) states is shown in Figure 1. The mechanisms affecting such changes are clarified in the subsections on neutralization and swelling of Carbopol.

All brands of Carbopol powder are hydrophilic and can absorb water from humid air or liquid water and such water-induced structural changes can be followed by the FT-IR (Szabo et al. 2011). In water dispersions, Carbopol particles can form large cross-linked structures, stabilized by four types of hydrogen bonds (Li et al. 2007; Tessarolli et al. 2014). It was suggested the Carbopol particle network is formed by structural units (Putz and Burghelea 2009), which are interconnected by fairly weak hydrogen bonds, and the units can be deformed and destroyed under shear. Since the structural units were undefined, the maximum size of a single, dry spherical Carbopol macromolecule can be estimated to be 410 nm using the maximum reported molecular weight of 4.5×10^9 Da (Lochhead 2017), mass of 1 Da of 1.66×10^{-27} kg, and bulk (minimum) density of 208 kg/m^3 (Panzade and Puranik 2010). On the other hand, using the low molecular weight of 3×10^6 (Gomez-Carracedo et al. 2004; Gomez et al. 2010; Muramatsu et al. 2000) and the true

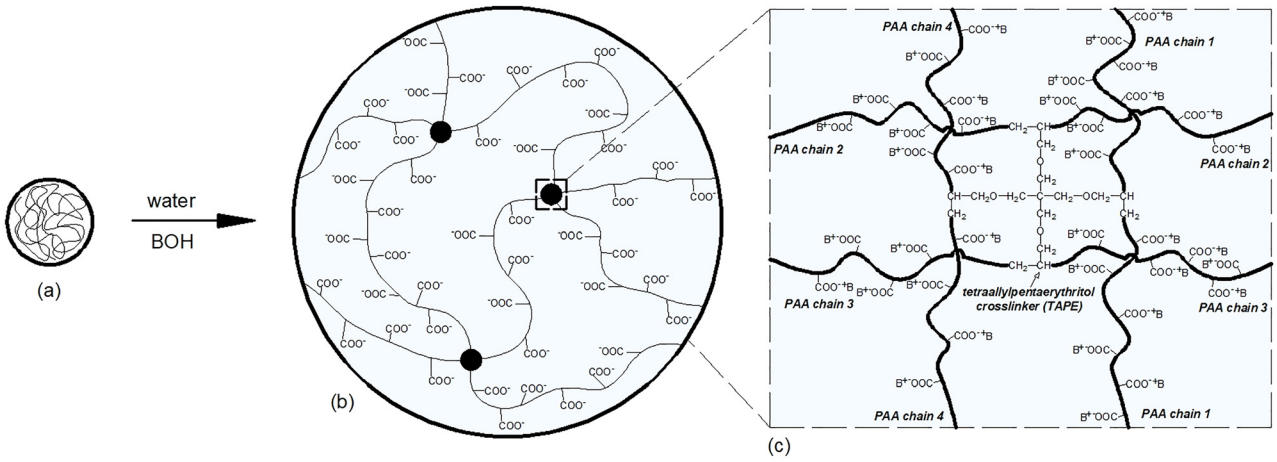

Figure 1: Schematic visualization of Carbopol particle.
(a) in solid state with COOH groups, (b) after neutralization in an alkali aqueous solution with dissociated COO^- groups where solid circles represent one particular cross-linked node shown in (c) in more detail.

density of 1410 kg/m^3 (Panzade and Puranik 2010) the minimum size of a Carbopol macromolecule can be estimated to be 19 nm. The estimated range of macromolecule size from 0.02 to 0.41 μm confirms that commercial, typical Carbopol particles are multimacromolecule agglomerates.

That conclusion can be supported by the microscopic photo of a Carbopol 934 particle shown in Figure 2(a) showing irregular network composed of small ingredients (Davies and Stokes 2008). A similar picture from cryogenic scanning electron microscope (cryo-SEM) is presented in Figure 2(b), which shows agglomerated microgel particles of Carbopol 974P of 100–300 nm in size to form a large particle of about 5 μm in size (Lefrancois et al. 2015).

2.5 Basic properties

Commercially available carbomers are in the powdery form, usually with polydispersed particles of 0.2–6.0 μm-size, which are formed of a large network of cross-linked molecules (Di Giuseppe et al. 2015). The glass transition temperature of solid Carbopol polymers is between 130 and 140 °C (Gomez-Carracedo et al. 2004). In the solid state, the polymer molecules are entangled, highly coiled, see Figure 1(a), and they start uncoiling when dispersed in water, especially after neutralization (Figure 1(b)) (Lochhead 2017; Shafiei et al. 2018). Carbopol particles suspended in water have dissociation constants expressed as pKa = 6.0 ± 0.5, with pH = 2.5–3.0 of 1% dispersion in water and are therefore classified as weak acids (Lubrizol 2008). The final formulation, of either percolated microgel structure in low concentrations of Carbopol (Gutowski et al. 2012) or jammed suspension at concentrations higher than about 0.08% wt. (Pemeja et al. 2019; Prasad et al. 2003), is obtained by neutralizing the carboxylic groups of a Carbopol suspension, usually with low-cost aqueous NaOH solutions. However, other inorganic (NH_4OH, KOH) or

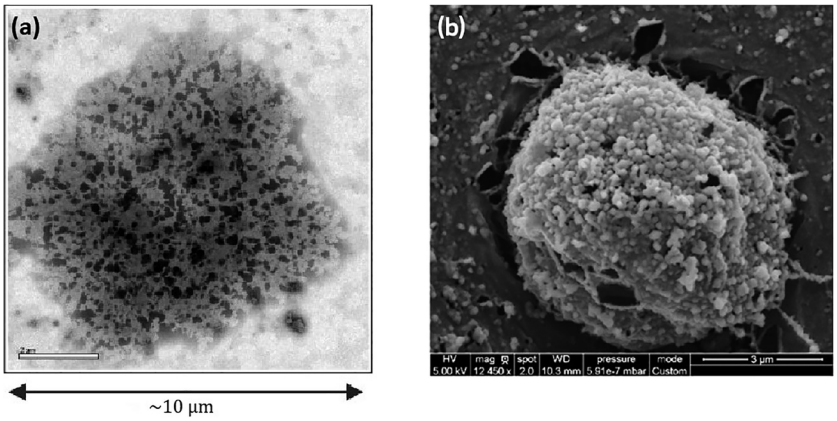

Figure 2: Images of Carbopol gel particles.
(a) microscopic [by permission of the *Journal of Non-Newtonian Fluid Mechanics* (Davies and Stokes 2008)]; and (b) cryo-SEM picture [by permission from Journal of Applied Polymer Science (Lefrancois et al. 2015)].

organic (amine-type) bases applied in liquid form or aqueous solution, can be used for neutralizing as well. The type of four bases used for neutralization of two Carbopol grades was found without impact on apparent viscosities of Carbopol microgels (Barry and Meyer 1979a; Berney and Deasy 1979; Dolz et al. 1998; Hernandez et al. 1998). Suggested base/Carbopol ratios for neutralization to obtain the pH value of 7 can be found in (Lubrizol 2009). After neutralization, PAA carboxylate groups get ionized making polymer chains largely uncoiled by electrostatic repulsion of $-COO^-$ groups (Lochhead 2017; Shafiei et al. 2018). As a result of neutralization, polyelectrolyte microgel particles can increase their dimensions by about 10 times and their volume by 200–1000 times (Lochhead 2017; Oppong and de Bruyn 2011; Rodriguez et al. 1994). Those microgel particles may be viewed as sterically stabilized particles without a core (Saunders and Vincent 1999). At a sufficient concentration of Carbopol microgel dispersion in water, swollen particles occupy most of the mixture volume and jamming can occur to particles pushing against their neighbors (Bonn et al. 2017; Coussot et al. 2009).

2.6 Formulation of Carbopol microgels

Preparation of hydrogels usually requires sufficient shearing of the mixture of powder and water to produce a homogenous dispersion of carbomers before and after neutralization. Typical devices used to disperse agglomerated particles in a solvent are stirred vessels or special colloidal mills. Carbopol concentrations of 0.1% and higher were recommended to get stable rheological characteristics (Kelessidis and Hatzistamou 2011). However, dissolved CO_2 should be carefully removed from the dispersion at low polymer content (Borrega et al. 1999). CO_2 affects pH and, in consequence, the dispersion rheology.

Literature reports on the morphology of dry and wet particles and on the impact of shearing intensity on Carbopol dispersions are only partly consistent. Two main microscopic techniques have been used in published studies on Carbopol particle morphology with the use of visible light and/or electron images. However, every microscopic analysis has specific imperfections in accurate reflection of the microgel structure. Light microscopy techniques have limited resolution and involve chemical labeling or contrasting (Kaberova et al. 2020). Typical electron microscopy (EM), either scanning (SEM) or transmission (TEM), require very deep vacuum (Egerton 2005). Moreover, the critical step in EM is obligatory solidification of hydrogel specimen by freezing or drying of analyzed specimens, which increases the risk of changes in sample morphology (Kaberova et al. 2020). Typical cryo-SEM images of neutralized Carbopol microgels showed honeycomb structures with pores of about 1–10 μm in size (Kim et al. 2003; Lefrancois et al. 2015; Piau 2007; Shafiei et al. 2018). Cryo-SEM fails to truly show the particle morphology due to evaporation of water (Shafiei et al. 2018). Environmental SEM (ESEM), contrary to the conventional and cryo-SEM, can give rise to artifact-free imaging of alginate hydrogels (Koch and Włodarczyk-Biegun 2020). Specimens in ESEM can remain wet surrounded with saturated water vapor due to relatively high pressure of a few hundred Pascal (Egerton 2005). Though a high-pressure, rapid freezing was claimed to avoid formation of ice crystals, the cryo-SEM pictures show spherical Carbopol particles (Lefrancois et al. 2015), which are different in form from those seen in light microscopy. Summing up, only light microscopy and carefully executed environmental SEM can lead to low artefact in microscopic analysis of hydrogels (Kaberova et al. 2020).

Evolution of particle size and shape during hydration (preneutralization) stage of Carbopol Ultrez 30 particles was visualized by means of the inverted light microscope Delta Optical IB-100 as presented in Figure 3, which was obtained by the authors. Four pictures, from (a) to (d), show Carbopol particles: just before contact with water (a), 5 s after coverage with water (b), after 20 s (c) and after 2400 s (d) from the start. A similar mesostructure of swollen Carbopol 940 microgel to that in Figure 3(d) was proposed by (Agarwal and Joshi 2019).

The white spots with associated shadows in photos (b) to (d) originated from particles floating on the specimen free surface. Mean diameters, $d_{2,1}$, of the particles were calculated as 10, 20, 22 and 25 μm for the hydration time of 0, 5, 20 and 2400 s, respectively. The hydration process was initially rapid, resulting in 2/3 of the total linear size increase within the first 5 s. Insignificant particle growth was noted after 2400 s. Visibility of the particle contours in water was decreasing during the hydration progress (a through *d*) and disappeared after particle neutralization (not shown). Similar loss of a clear border between neutralized particles and water was reported in other studies when direct fluorescent dyeing was used in confocal microscopy (Gutowski et al. 2012; Younes et al. 2020a). Nevertheless, specific dyeing allowed to visualize swollen Carbopol particles under confocal microscope (Dinkgreve et al. 2018a; Géraud et al. 2017; Lefrancois et al. 2015; Younes et al. 2020b). Photos (a) and (b) of Figure 4 present such images of Carbopol Ultrez 10 particles dyed with fluorescent Rhodamine 6G, respectively for normally prepared microgel at pH = 7 and strongly stirred, and (c) shows corresponding particle size distributions (PSD) (Dinkgreve et al. 2018a).

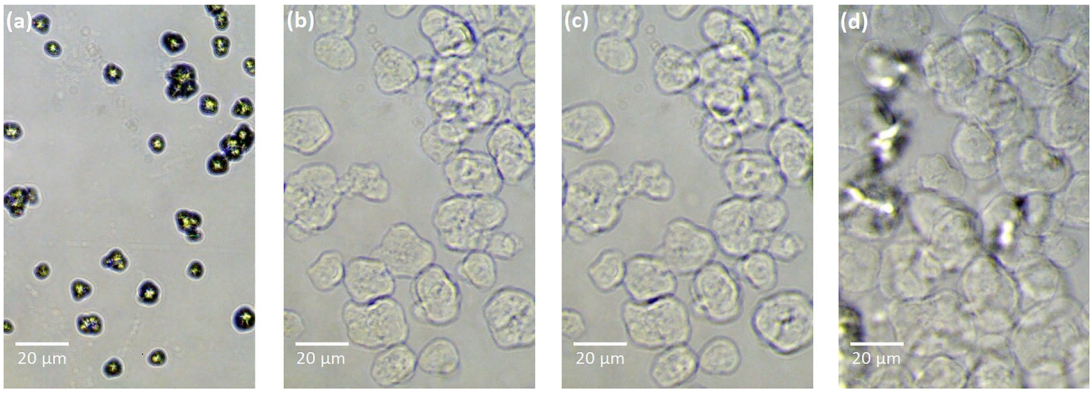

Figure 3: Time evolution of Carbopol Ultrez 30 particles during hydration stage observed in light microscopy. (a) at the start 0 s, (b) after 5 s, (c) after 20 s and (d) after 2400 s.

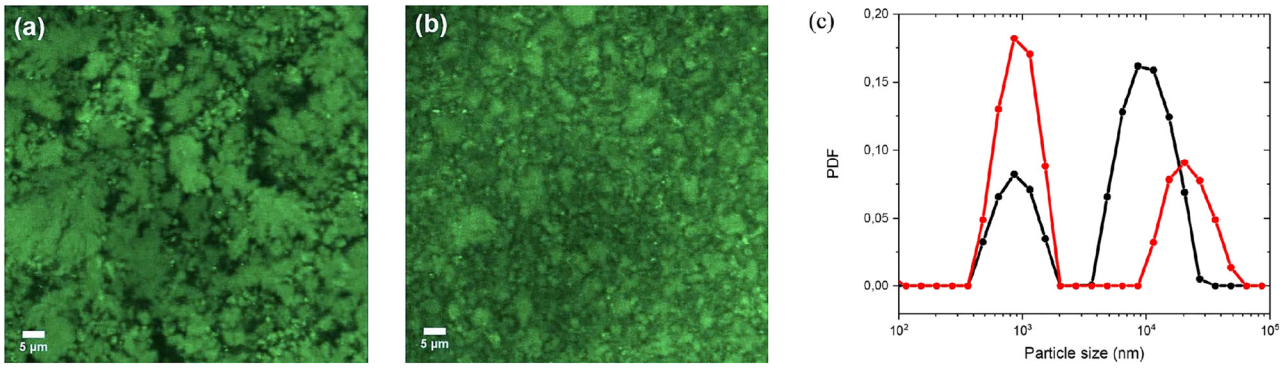

Figure 4: Confocal microscope images of Carbopol microgel. (a) normally stirred and (b) strongly stirred, with PSD in (c) where black line is for normal Carbopol and red line represents highly-stirred Carbopol. The white bar in (a) and (b) is 5 µm long. Reproduced from (Dinkgreve et al. 2018a), with the permission of the Society of Rheology.

Techniques of static and dynamic light scattering were also applied to evaluate distribution of Carbopol dispersions, both in hydrated and fully swollen state (Gutowski et al. 2012; Lee et al. 2011; Piau 2007; Rodriguez et al. 1994). Significant polydispersity was found for different grades and concentrations of Carbopol. Particle size distribution was usually two-modal with its maxima of the order of 1 and 10 µm, like the distributions shown in Figure 4(c).

The effect of varied mixing intensity of three EDT Carbopols on their rheology characteristics was found insignificant in early studies (Dolz et al. 1998; Hernandez et al. 1998). Similarly, very small differences of the yield stress and G' and G'' moduli were recently found between mildly and strongly stirred 0.2% Carbopol 980 (Bhattacharjee et al. 2018). Laser diffraction granulometer was applied to measure bimodal size distribution of Carbopol 5984 particles subjected to 5 levels of turbine stirrer speed prior to neutralization (Baudonnet et al. 2002). The authors found the $D_{3,2}$ mean particle size almost linearly decreased from 15 to 4 µm as a result of up to three-fold increase in stirrer speed. Subsequent neutralization of those five Carbopol dispersions resulted in lowering the apparent microgel viscosity with growing stirring intensity. Interestingly, almost direct proportionality was found between the microgels and non-neutralized dispersions of the same stirring intensity (Baudonnet et al. 2002). Associated authors carried out a similar study for two other Carbopol types and obtained qualitative agreement with the former study (Baudonnet et al. 2004). The application of confocal fluorescent microscope to dyed samples of 0.6% Carbopol Ultrez 10, either normally (50 rpm) or strongly (2000 rpm for 20 h) stirred, revealed bimodality of both microgels with a higher proportion of small particles of about 1 µm in size and mild thixotropy of the strongly stirred microgel (Dinkgreve et al. 2018a).

In order to obtain homogenous suspensions, dispersing equipment should generate shear stress high enough to separate individual particles that are not

chemically bonded. It is therefore essential to estimate the threshold shear stress, beyond which damage could be done to the polymer molecules sheared. The breaking stress of chemical bonds within a carbomer molecule can be assessed based on their bond energies. The bond energy of typical carbomer bonds is approximately 85 or 100 [kcal/mol], respectively for the C–C and C–O or C–H (Blanksby and Ellison 2003). Those values correspond to $(6–7) \times 10^{-19}$ [J] for a single molecule. Though the energies were measured in the gas phase, the polymer-solvent solvation effects in the liquid phase are relatively small (Blanksby and Ellison 2003). Assuming further that the separation distance of two atoms to result in bond breakage is of the order of 1 nm and the average diameter of a nonswollen carbomer molecule is about 30 nm, the threshold shear stress exerted on the molecule can be estimated as $\sigma_{th} = 70$ [MPa]. That threshold value is rather high and roughly equal to the tensile strength of solid polymers (Sperling 2006). For a swollen molecule, the estimated breakage shear stress yields even a higher value. In conclusion, typical shear stresses applied in the process equipment of a few kPa cannot cause breakage of chemical bonds in Carbopol macromolecules.

2.7 Carbopol dissociation

From the chemical perspective, it is important what ratio of the carboxylic groups, –COOH, of a carbomer polyacid gets ionized and dissociated. Titration experiment is one of the simplest and most useful ways of determination of the dissociation extent (Borukhov et al. 2000). Although the degree of polyacid dissociation depends on the extent of neutralization, the detachment of hydrogen ions occurs mainly at unlinked ends of polymer chains (Kawaguchi et al. 1995). Experimental results of Carbopol titration are presented in the next subsection describing neutralization of polyacids. In the quantitative description of the dissociation (neutralization) process of acidic polyelectrolytes, the following dissociation of monomeric –COOH groups is considered (Borukhov et al. 2000; Kawaguchi et al. 1995),

$$–\mathrm{COOH} \overset{K}{\rightleftarrows} – \mathrm{COO^-} + \mathrm{H^+} \tag{2-1}$$

coupled with the neutralization reaction of hydrogen and hydroxyl ions,

$$\mathrm{H_2O} \rightleftarrows \mathrm{H^+} + \mathrm{OH^-} \tag{2-2}$$

with the latter originating from a strong base, e.g., NaOH. The dissociation (ionization) degree, α, in polyelectrolyte titration is usually defined as the ratio of the molar concentration of dissociated carboxylic groups, $[–\mathrm{COO^-}]$, to the initial concentration of –COOH expressed as the sum of the current molar concentrations of the undissociated, [–COOH], and dissociated, $[–\mathrm{COO^-}]$ carboxyl groups of the polyion analyzed (Borukhov et al. 2000; Kawaguchi et al. 1995).

$$\alpha = \frac{[–\mathrm{COO^-}]}{[–\mathrm{COOH}] + [–\mathrm{COO^-}]} \tag{2-3}$$

The average degree of dissociation of monomers is related to the negative logarithm of hydrogen ions, $\mathrm{pH} = -\log_{10}[\mathrm{H^+}]$, and the thermodynamic dissociation constant, K. For low concentrations of the species of Eq. (2-3), their thermodynamic activities may be approximated by relevant molar concentrations and analogously, the K activity constant approximated by the apparent K_a defined in Eq. (2-4).

$$K_a = \frac{[–\mathrm{COO^-}]\,[\mathrm{H^+}]}{[–\mathrm{COOH}]} \tag{2-4}$$

Using a logarithmic expression for K_a as $pK_a = -\log_{10} K_a$, and transforming Eqs. (2-4) and (2-3) one gets:

$$\mathrm{pH} = pK_a - \log_{10}\frac{1-\alpha}{\alpha} \tag{2-5}$$

a form of the Henderson–Hasselbach equation with an inflection point at $\alpha = 0.5$ where $pK_a = \mathrm{pH}$. Following the van't Hoff relationship, the (2-1) reaction constant, K, can be approximated by the apparent K_a value calculated from Eq. (2-6) using the standard chemical potential (molar Gibbs energy), $\Delta\mu^0$, of reaction (2-1) in the absolute temperature, T.

$$K_a \cong \exp\left(-\Delta\mu^0/RT\right) \tag{2-6}$$

However, it was found for microgels of three Carbopol brands that their K_a significantly depended on the dissociation degree (Testa and Etter 1972, 1974), i.e., the standard chemical potential of Eq. (2-1) depended on the extent of neutralization of the reacting macroions. The pK_a values for dissociation of the first $\mathrm{H^+}$ ion from the macromolecule, pK_{int}, were estimated to be 7.1, 7.1, 6.9 respectively for Carbopol 934, 940, 941 (Testa and Etter 1972), which confirms the fact that Carbopols are weakly acidic compared to acrylic acid. The fraction of dissociated (charged) monomeric units of poly(acrylic acid) was determined by application of sodium-selective electrode to measure activity of $\mathrm{Na^+}$ ions during titration with NaOH (Konop and Colby 1999).

2.8 Polyacid neutralization

Another parameter used in polyelectrolyte titration is the degree of neutralization, y, defined as a concentration ratio of the added strong base, $[c_B]$, to the monomeric units of molar concentration (Borukhov et al. 2000; Curran et al. 2002).

$$y = \frac{[c_B]}{[-\mathrm{COOH}] + [-\mathrm{COO}^-]} \tag{2-7}$$

A typical titration curve for strong acids, pH = $f(\alpha)$, has an S-shape with a sudden jump of pH at α = 1.0 whereas weak acids, e.g., polyacids, have the function line of pH vs. α of an inclined S-shape (Borukhov et al. 2000; Curran et al. 2002). A polyelectrolyte titration model was proposed and a satisfactory prediction of the pH and ionic strength effects on the polyion ionization relative to experiments was found (Michaeli and Katchalsky 1957). The authors derived the dependence of pH inside and outside polyions based on the Donnan equilibrium. The Donnan equilibrium is the thermodynamic equilibrium between two ionic solutions separated by a semipermeable membrane.

Titration was regarded as the best available method for exploring chain distribution in microgels (Hoare and Pelton 2008). Ionization of carbomer chains occurs mainly at their free ends, hence to enable the neutralizing base ions to diffuse to the core of some microgel particles and attain equilibrium, a slow titration should be applied preferably under a nitrogen atmosphere (Hoare and Pelton 2008). One can conclude that the titration methodology of polyacids is well established and proven. However, systematic titration data for Carbopol types have not been found in the open literature. Based on the patent description (Hsu 1997), one can safely assume that the weight ratio of the cross-linking agent to acrylic acid in Carbopol types is close to 1%. This allows to accept with fair accuracy the molar concentration of the –COOH groups per unit mass for homopolymeric type of Carbopol the same as in acrylic acid.

Figure 5 shows titration curves for two brands of Carbopol and the poly(acrylic acid). A typical feature of the pH vs. y relationship for polyacids is slow increase of pH for the degrees of neutralization, y, further from y = 1 where a sudden jump occurs. The pH values for monomeric organic acids are lower for $y < 1$ and higher for $y > 1$ than those of their polymers (Borukhov et al. 2000), cf. Figure 5. The higher polyacid concentration, the closer pH to that for the monomeric acid and their titration lines collapse at y = 1. This implicates inhibiting action of neighboring carboxyl groups on dissociation of the other in carbomers. In the case of strong salt added and a constant polyacid concentration, a higher salt concentration lowers the pH values (Borukhov et al. 2000).

Neutralization of carbomers results also in changes in the ionic strength of dispersion. The equivalent conductivity decreases with increase in the unneutralized carbomer concentration, contrary to partly or fully neutralized suspensions. With growing concentration of Carbopol 940 microgel, the conductivity of fully neutralized dispersions first slightly decreases to a minimum at about 0.05% wt. and then increases (Testa and Etter 1976). The minimum conductivity was associated with the transition from Newtonian to shear-thinning rheology of the Carbopol dispersion studied (Testa and Etter 1976). It results from disappearance of free H^+ ions, which is typical for weak polyelectrolytes (Kawaguchi et al. 1995). Similar conductivity minima were also found for other microgels containing carboxylic groups (Hoare and Pelton 2004).

2.9 Osmotic pressure

Polyacid strands represent negatively charged macroions and are therefore electrostatically stretched, moreover, the electrostatic repulsion prevents them from aggregating. Macroions attract small counterions (microions) and also molecules of a polar solvent, such as water, forming a swollen microgel particle. The accumulation of counterions in the vicinity of charged strands generates osmotic pressure between the macroparticle and surrounding polar solvent (Dobrynin 2008). Osmotic pressure can be regarded as the mean normal stress (Seth et al. 2006). Balance between the osmotic pressure of free counterions and internal elasticity of the microgel particle determines the

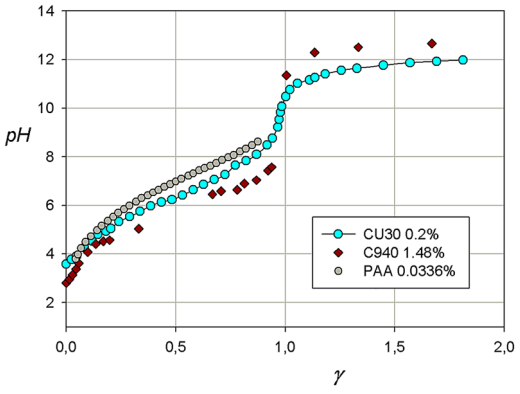

Figure 5: Dependence of polyacid neutralization degree on pH for: 0.2% Carbopol Ultrez 30 (CU30, own results), 1.48% Carbopol 940 (Curran et al. 2002), (C940), 0.0336% poly(acrylic acid) (Sakurai et al. 1993), (PAA).

extent of particle swelling (Nisato et al. 1996). In the fully swollen polyelectrolyte microgel at equilibrium, the osmotic pressure, π, is equal to the shear modulus, G, in the low limit of salt concentration (Rubinstein et al. 1996):

$$\pi = G \tag{2-8}$$

At very low salt concentrations, the osmotic pressure is directly proportional to the polyelectrolyte concentration, c, and approximately equals the thermal energy (kT) per free counterion:

$$\pi \cong \frac{c}{A} kT \tag{2-9}$$

where the parameter $A > 1$ accounts for the counterion condensation.

The total osmotic pressure, π, of a polyelectrolyte microgel comprises four components that describe the effects of: solvent-polymer mixing entropy, π_m, polymer network elasticity, π_{elast}, the Donnan equilibrium of ion charges, π_D, electrostatic interactions within and outside polyions, π_{elec}, due to dissociation (Hoare and Pelton 2007).

$$\pi = \pi_m + \pi_{\text{elast}} + \pi_D + \pi_{\text{elec}} \tag{2-10}$$

The first two components, π_m and π_D, favor swelling, π_{elast} promotes deswelling whereas the charge interactions term, π_{elec}, acts either positively or negatively depending on the salt counterion amount added to Carbopol dispersion. Let us notice the counterion concentration is much higher inside than outside microgel particles due to electrostatic attraction of the charged polyion. Therefore, the particles are almost electro-neutral locally and globally as well (Borrega et al. 1999). Romeo et al. (2012) expressed details of the first two terms of the right side of Eq. (2-10) based on the Flory theory of polymer gels. The authors found the counterion fraction $\Gamma = 0.022$ outside the polyelectrolyte, which confirms that almost all counterions are trapped inside the polyion particle. Four components of the microgel osmotic pressure, essentially similar to those in Eq. (2-10), were analyzed by Li et al. (2014) who developed new quantitative relationships for the components. Two important papers on the osmotic pressure and microgel swelling were published in 2016 and their results are commented in the section on micromechanical models (Denton and Tang 2016; Rumyantsev et al. 2016).

2.10 Microgel swelling

Microgel particles exhibit stimuli-responsive nature of their reversible volume transition in response to changes in pH, ionic strength, shear, temperature, solvent and external electromagnetic field (Tan and Tam 2008). Both experimental and theoretical attempts were undertaken to quantify how the osmotic pressure of macroions influences their swelling abilities. Fundamentals of the swelling theory of cross-linked polymers were provided by Flory and Rehner (1943). Direct application of the theory to describe swelling of responsive microgels led to an advanced approximation of the Flory parameter (Nigro et al. 2017).

Michaeli and Katchalsky (1957) defined the degree of microgel swelling as relative molar fraction of polymethacrylic acid microgels prior to and after neutralization. Their model predicted well the dependence of the swelling degree on pH and salt concentrations in the microgel. Perhaps the first comprehensive study of Carbopol swelling, for different microgel concentration and ionic strength, was published by Taylor and Bagley (1974). The authors used centrifuge data to determine the swelling extent, Q, expressed as the weight ratio of swollen microgel, W_s, to dry polymer, W_d, Eq. (2-11). They found a linear dependence of the reciprocals of Q and the ionic strength of the Carbopol microgels.

$$Q = \frac{W_s}{W_d} \tag{2-11}$$

The Carbopol microgel volume fraction in suspension, ϕ, was estimated from viscosity measurements as a measure of microgel swelling (Carnali and Naser 1992), which strongly depended on ionic strength. Their results were in semi-quantitative agreement with earlier ones (Taylor and Bagley 1974). Other authors proposed a simplistic core–shell model and used experimental data from light scattering to express swelling in terms of the particle radius of gyration (Rodriguez et al. 1994). A theoretical study of swelling of single polyelectrolyte chains and those in microgels was carried out by Kramarenko et al. (1997) who stressed the role of counterion division between the polymer and solution. A simple relationship linking microgel volume fraction, ϕ, with volume swelling ratio, $\tilde{Q}$, weight ratio of polymer to dispersion, C, molar volume of monomeric units, V_m, molar concentration of collapsed polymer particles, c_0, and the density ratio of dispersion, ρ_s, to that of polymer, ρ_p, was given in Eq. (2-12) Cloitre et al. (2003b).

$$\phi = \frac{\tilde{Q}C}{V_m c_0} \frac{\rho_s}{\rho_p} \tag{2-12}$$

They found that water dispersions of polyion particles stop flowing at low shear stresses when their volume fraction reaches the value of $\phi_m = 0.64$ that corresponds to that for close-packing of hard-sphere dispersions.

Drozdov et al. (2015, 2016) made a significant progress in modeling of equilibrium swelling of anionic hydrogels, which were considered as elastic three-phase media; solid polymer, water solvent and mobile ions as a solute. The effects on microgel swelling of pH and ionic strength compared very well with experimental results for varied pH and salt concentration, after fitting material constants of the models (Drozdov and Christiansen 2015). Another approach, which does not require adjusted parameters was proposed to model the swollen state of charged polyelectrolyte microgels (Rumyantsev et al. 2016). Three position types of counterions relative to the polyion chain are considered in the model; i) counterions accumulated close to the chain, called Manning-type condensation, ii) paired (bonded) counterions with chain ions, iii) a small amount of counterions freely located in the solution surrounding polymer particles. The model allows to predict microgel swelling and conductivity of polyelectrolyte dispersions. Following similar earlier models (Khokhlov and Kramarenko 1996; Kramarenko et al. 2006; Marcus 1955), the model of Rumyantsev et al. (2016) assumes the total free energy of interactions, F, between the charged polyelectrolyte and surrounding solution with ions and consists of five components: chain elongation/compression, F_{el}, volume interaction in the Flory-Huggins form, F_{FH}, translational entropy of counterions in both condensed regions, F_{tr}, electrostatic energy of the model polyion-counterion cylinders, $F_{el\text{-}st}$, and aggregation energy of ion pairing, F_{agg}.

$$F = F_{el} + F_{FH} + F_{tr} + F_{el-st} + F_{\text{agg}} \tag{2-13}$$

Minimization of the F function with respect to the distance between nearest-neighbor cross-link and the fraction of free counterions allows to derive the equilibrium microgel volume. Although the applicability of the model was tested for three cross-linked polyelectrolyte microgels, it has not been tested yet for Carbopol microgels (Rumyantsev et al. 2016).

2.11 Processing of carbomer microgels

Chemical engineers have been involved in designing process equipment for yield-stress fluids, applying the classic empirical approach and also the methods of Computational Fluid Dynamics, CFD. One of industrially relevant problems is the fluid-fluid displacement of Carbopol microgels from pipes of varied angle of inclination, which was experimentally studied (Alba et al. 2013; Taghavi et al. 2012). Three unsteady regimes of the two-fluid flow were established: slump, center-type and turbulent/mixed. Homogenization of Carbopol dispersions can be achieved either in stirred tanks or/and in in-line mixers. Experiments with such microgels in agitated vessels were associated with the determination of impeller power consumption, local velocities and cavern (well-mixed zone) sizes (Amanullah et al. 1997; Cortada-Garcia et al. 2018; Curran et al. 2000; Story and Jaworski 2017). Such studies resulted in well-established correlations for calculating power draw and cavern sizes for a range of impellers for stirring of Carbopol microgels. Mixing performance for Carbopol 940 microgel with glycerol was investigated using laser induced fluorescence and both well and poorly mixed zones were found (Alberini et al. 2014; Cortada-Garcia et al. 2018). Carbopol microgel was also used in pipe heat transfer investigations in the laminar, transitional and turbulent flow conditions (Peixinho et al. 2008). Using the linear velocity profile inside the thermal boundary layer and the Herschel-Bulkley rheology, the authors' experimental data conformed to literature correlations derived for heat transfer in Newtonian fluids with two correction factors. One factor was for non-Newtonian behavior and another one for the thermo-dependency of the microgel consistency. Carbopol microgels were also applied as model yield-stress fluids, in particular for predicting cavern size in opaque liquids, such as paper pulp (Curran et al. 2002; Ovarlez et al. 2013).

The CFD numerical methods are based on the principles of mass, energy and momentum transport developed in fluid mechanics. One of the first numerical approaches to predict 3D flow of a yield-stress fluid in a stirred tank was published by Arratia et al. (2006). Their predictions for 0.1% Carbopol 940 with measured yield stress of 1.2 Pa captured essential features of experimental PIV observations, including stagnation regions outside well-mixed caverns. Formation of caverns in stirred yield-stress fluid was well predicted for the laminar flow of 0.1% Carbopol 940 of 1.2–2.6 Pa in yield stress, although with less accuracy for higher flow intensities (Adams and Barigou 2007). Two authors of the present paper carried out CFD modeling of momentum transfer in stirred tanks for a 0.2% Carbopol 940 dispersion (Dylak and Jaworski 2014; Story and Jaworski 2017). The authors successfully validated simulated velocity fields and also concluded that the cavern volume corresponds to the primary circulation zone in stirred tanks. A 1% wt. Carbopol 940 dispersion of 131 Pa yield stress was used in a joint PIV and CFD investigation on a creeping flow around an adhesive square plate (Ahonguio et al. 2016b). Again, a good agreement between the velocity field from experiments and simulations was achieved for that elasto-viscoplastic fluid. Moreover, three rheological types of fluid, including a 0.2% Carbopol 980

microgel of 35Pa yield stress, were used in CFD modeling of coupled fluid flow and heat transfer in a scraped wall tube exchanger (Yataghene and Legrand 2013). Numerical predictions compared favorably with published literature data. Another successful application of CFD to model the flow of Carbopol 940 microgel in a microchannel was recently published (Liu et al. 2018). To recap this section one may conclude that flows of Carbopol microgels with a broad range of yield stress were effectively simulated in process equipment by means of CFD tools.

2.12 General remarks

In the summary of the chemical characterization of Carbopol microgels, the following remarks can be made. Carbomers are lightly cross-linked polymers of acrylic acid, which have very high molecular weights well above a million of Daltons. A variety of available carbomers differ in polymerization conditions that are tailored to specific applications. Commercial Carbopols have particles of micrometer-range size and are usually multimodal. Their aqueous dispersions are lightly acidic and produce translucent microgels after neutralization with inorganic or/and organic bases. The stretched polyions attract cations and water dipoles and form swollen hydrogels. Stability of those dispersions results from the repulsive forces between charged particles and internal balance between the chain elasticity and osmotic force mainly caused by positively charged counter-ions. Thus, the properties of a Carbopol microgel can be stimulated by chemical and physical conditions such as pH, ionic strength, temperature, solvent and external electrical force. Theoretical description of forces acting on polyelectrolyte particles has already been well developed. Those theories quantitatively explain swelling conditions of microgels. The design foundations of microgel process equipment reached the stage of intermediate maturity from the view of both experimental correlations and numerical modeling. In general, the chemical structure and properties of carbomer polyelectrolyte microgels determine their physical and rheological characteristics, which are presented in the two following sections.

3 Physical models of Carbopol microgels

From a variety of physical tools for characterization of Carbopol microgels, mesoscopic models were chosen to be included in this Section. Following a brief introduction, three microgel-specific models are described: jamming, micromechanical and polyelectrolyte, respectively.

3.1 Introduction to physical modeling

From the physical perspective, two key types of yield-stress materials can be distinguished: soft glasses and gels since each material exhibits different solid-fluid phase transitions (Bonn et al. 2017). Soft glasses consist of deformable particles dispersed in a solvent and the particle volume fraction is well above close-packing (Bonnecaze and Cloitre 2010). The term “gel” is typically applied to low volume fraction dispersions of attractive colloids (Sciortino 2002), which narrows the phenomenological definition (Almdal et al. 1993). The physical modeling tools, which are applicable to microgels, consider the properties and structure of soft materials on the mesoscopic scale, that is of the order of a fraction of millimeter down to a fraction of micrometer. Aqueous dispersions of carbomers usually contain polyelectrolyte particles both below and above 1 μm in size and therefore they can be ranked neither as single-phase solutions nor as typical colloidal gels.

Soft materials exhibit elasto-hydrodynamic interactions mediated by the solvent. At an increased volume fraction of such particles, a colloidal glass phase can be formed (Pusey and Vanmegen 1986, 1987). The state results from metastable dynamic arrest of particles (Mattsson 2016; Pusey and Vanmegen 1987; Sollich 1998). That effect was attributed first by Ball and Melrose (1995) to particle jamming. Microrheological studies also supported the conclusion that jamming in microgels is similar to the behavior of glassy liquids (Nordstrom et al. 2010a). It was also proposed that concentrated Carbopol dispersions can be regarded as glasses of individual elastic sponges with the extent of interparticle contacts growing with their concentration (Piau 2007). Other microrheological experiments confirmed the yield stress is a result of jamming of Carbopol particles (Oppong and de Bruyn 2011). Ikeda et al. (2012) analyzed numerically both microscopic and macroscopic dynamics of soft repulsive particles. Their simulations showed a similar type of rheological flow curves of colloidal glass transition to those of jamming transition. While thermal fluctuations play the main role in the glass transition, viscous dissipation dominates in the jamming. However, the critical solid-fluid volume fraction was to be different for the glass transition, $\phi_G \cong 0.58$ for perfectly hard spheres, from that of jamming transition, $\phi_J \cong 0.64$. Incidentally, the crossover was also studied experimentally (Dinkgreve et al. 2018b). A rheological model was proposed for the glass-to-jamming crossover

in flow curves (Ikeda et al. 2012). The model assumes that the total stress is a sum of three contributions from the glass, jamming and solvent.

A more fundamental problem whether solids do flow was theoretically considered with the conclusion that solidity is time-depended, which explains the apparent yield stress as an ultra-slow motion in rheological studies (Sausset et al. 2010). Carbopol dispersions may also contain submicron particles, which contribute to aging due to thermal fluctuations. However, slow aging effects can be partly reversed by prior shear flow causing "shear rejuvenation," which can be applied in rheological flows (Cloitre et al. 2003b). Thus, reproducible rheological measurements below the yield stress require perfect control of both the preparation and stress history of the material studied (Cloitre et al. 2000). The elastic modulus, G', of the solid hair gel increased logarithmically with time of the gel rest, t_w (Coussot et al. 2006).

$$G = \kappa \ln\left(\frac{t_w}{t_0}\right) \tag{3-1}$$

A recent study also suggested that Carbopol microgels exhibit physical aging with weak enhancement of the elastic modulus (Agarwal and Joshi 2019). However, at present we are still far from understanding microscopic processes of aging and rejuvenation (Agarwal and Joshi 2019; Mendes and Thompson 2019).

Many different types of theoretical models were published for fluid-amorphous solid systems, such as Carbopol dispersions in water, to account for the complex rheology of yield-stress materials, (e.g., Bonn et al. 2017; Voigtmann 2014). At present, however, a complete first-principle theoretical approach does not exist (Bonn et al. 2017). In this paper, three types of physical modeling are chosen for quantitative description and they focus on the properties of microgels and similar substances. The most popular models for microgels analyze the yield-stress materials as jammed dispersions or micromechanical systems. In addition to the two models, physical polyelectrolyte approaches are also described here. The soft glassy rheology model should be also mentioned as an important representative of physical models (Sollich 2006; Sollich and Cates 2012). A deficiency of the SGR model consists in the assumption that local elastic properties are homogenous in soft glasses (Sollich 2006), whereas microgels are heterogeneous in the microscale.

3.2 Jamming dispersions

It was experimentally found for a yield-stress Carbopol microgel the material was inhomogeneous since some submicron-scale suspended tracer particles were diffusive while others remained immobilized between larger microgel particles (Oppong and de Bruyn 2007). That observation was supported by other authors (Dinkgreve et al. 2018a; Gutowski et al. 2012), who used confocal fluorescence microscopy and detected significant void parts between microgel particles of different Carbopol types. Further experimental results implied the yield stress of Carbopol microgels appears as the result of jamming of microgel particles (Oppong and de Bruyn 2011). Likewise, the characteristic change in dependence of rheological parameters on the Carbopol concentration was interpreted as an onset of jamming of swollen polymer molecules (Weber et al. 2012). Nevertheless, to maintain the jamming mechanical equilibrium, a sufficiently large number of inter-particle contacts is required and the particle facets are flat at contact (Seth et al. 2011). In addition, due to the absence of significant thermal fluctuations, the preparation stage of soft materials controls location of the jamming transition (Bonn et al. 2017).

Dinkgreve et al. (2018b) investigated the flow curves of thermal and athermal particle dispersions of different volume fractions, ϕ. They found curves for yield-stress fluids exhibited scaling with respect to either the glass or jamming fraction, ϕ_G or ϕ_J. Following the additive idea of the glass and jamming physics of Ikeda et al. (2013), the flow curves were scaled onto a single universal flow curve, regardless of the type of interparticle interactions (Dinkgreve et al. 2018b). However, it was also suggested that some of the used microgels might not have been fully athermal (Bonn et al. 2017).

An attempt to disentangle the jamming and glass physics of dense soft materials was undertaken by Ikeda et al. (2012, 2013). The authors proposed an additive momentum model of random motion of harmonic elastic spheres, which represent individual soft particles. The repulsive particle interaction energy, ε, was used as a key material parameter. The ratio of the thermal energy of a molecule, k_BT, to the particle interaction energy was considered to be the measure of particle softness.

$$\frac{k_BT}{\epsilon} = \frac{t_r}{t_0} = \frac{\tau_0}{\tau_r} \tag{3-2}$$

That energy quotient also represents a ratio of the time scales for energy dissipation for structural relaxation, t_r, to that of the microscopic Brownian motion, t_0. It is also equal to the ratio of the stress scales for thermal fluctuations, τ_o, and the athermal strain, τ_r. At low values of particle softness, their model allowed to distinguish between the glass transition for Brownian soft particles and the jamming transition for larger particles (Ikeda et al. 2012, 2013). Contrary to the

glass transition, thermal fluctuations play no role in the jamming transition (Bonn et al. 2017). Two rheology regimes were established using the products of one of the two times and the flow rate, $\dot{\gamma}$: glassy regime for $t_0\dot{\gamma} \ll 1$ and jammed regime for $t_r\dot{\gamma} \geq 1$ (Voigtmann 2014).

Detailed investigations of flow curves of a thermoresponsive yield-stress material around the jamming transition enabled to establish rules of curve universality Nordstrom et al. (2010a). A similar approach was applied by Dinkgreve et al. (2015). All flow curves of the shear stress, τ, vs. shear rate, $\dot{\gamma}$, were rescaled and resulted in a single master curve of $\tau/|\Delta\phi|^{\Delta}$ vs. $\dot{\gamma}/|\Delta\phi|^{\Gamma}$, where $|\Delta\phi| = |\phi - \phi_J|$ and $\phi_J \cong 0.64$. To explain the physical meaning of the scaling approach, a simple heterogeneous microscopic theory was applied. The theory was successfully validated with experimental data for four materials, including a Carbopol microgel, with $\Delta \cong 2.04$ and $\Gamma \cong 3.80$ (Dinkgreve et al. 2015). Similar exponent values of $\Delta = 2.13$ and $\Gamma = 3.84$ were reported for jammed emulsions in other studies (Dekker et al. 2018; Paredes et al. 2013).

3.3 Micromechanical models

Construction of a micromechanical model for polyelectrolyte dispersions was preceded by joint experimental studies of research teams collaborating with Cloitre (Borrega et al. 1999; Cloitre et al. 2003b; Meeker et al. 2004a, 2004b). They investigated a range of rheological properties of concentrated polyelectrolyte dispersions, which were designated as soft particle pastes. The authors studied concentration effects of the microgels on glass transition (Borrega et al. 1999), universal scaling behavior of their rheological characteristics using the experimental relaxation time of the millisecond range (Cloitre et al. 2003b) and the slip of flowing soft pastes near smooth surfaces (Meeker et al. 2004a, 2004b). Owing to simultaneous measurements of the local flow profiles of sheared microgels and of their rheological characteristics, in both smooth and rough cone-plate systems, it was found the slip was present only in the smooth system with the characteristic slip velocity, V_s^*, of an almost constant value (Meeker et al. 2004b). This was confirmed at and above the yield stress, with V_s^* being weakly dependent on the microgel concentration. The slip velocity value was found directly proportional to the storage modulus, G_0, and to the particle radius, R, and inversely proportional to the solvent viscosity, η_s.

$$V_s^* \cong G_0 R/\eta_s \tag{3-3}$$

The storage modulus corresponds to the plateau of low-frequency elastic modulus. An elastohydrodynamic lubrication model was also proposed to explain the microgel slip (Meeker et al. 2004b). In the elastic solid range, i.e., for $\dot{\gamma} < \dot{\gamma}_y$, the slip velocity, V_s, depends on the square of the shear stress, τ, according to the proportional relationship (3-4).

$$V_s/V_s^* \cong (\tau/\tau_y)^2 \tag{3-4}$$

The exponent 2 in Eq. (3-4) was found to be valid only for a microgel weakly adhering to solid surface, whereas for nonadhering surfaces the slip velocity varied nearly linearly with the shear stress (Seth et al. 2012). It was found that a slip yield stress, $\tau_s < \tau_y$, appeared when a smooth cone-plate system was used at very low shear rates. In a later study the slip yield stress was related to short-range forces between particles and the wall and the interaction was incorporated in their elastohydrodynamic lubrication model (Seth et al. 2008). When the net interaction wall-particle is repulsive, the wall is covered with solvent and then $\tau_s = 0$. A nonzero value of the slip yield stress occurs for attractive force when particles stick to the wall.

A micromechanical model was also presented by Seth et al. (2006). Their model quantitatively describes elastic properties of concentrated microgels and emulsions. Those materials were considered to be soft pastes composed of elastic spheres that were randomly packed above the random close-packing density of hard spheres. Similar reasoning enabled the authors to derive osmotic pressure and the shear modulus of microgels (Seth et al. 2006). The equation set of the micromechanical model was incorporated in dynamic molecular-like simulations and the model was widely validated against experimental data for microgels. The authors argue their model predictions of elastic properties of microgel particles confirm the link between the particle microstructure and their macroscopic properties.

Following an earlier proposal developed for other soft materials (Cloitre et al. 2003a), a universal modification, Eq. (3-5), of the Herschel-Bulkley relationship was recommended for soft glasses (Bonnecaze and Cloitre 2010). It was proposed to rationalize the rheological flow curves of soft glasses in the form of a master curve of the Herschel-Bulkley (H-B) type:

$$\frac{\tau}{\tau_y} = 1 + K\left(\frac{\eta_s\dot{\gamma}}{G_0}\right)^m \tag{3-5}$$

where the coefficient K is dependent on the microgel type, η_s stands for the solvent viscosity, G_0 for the low-frequency storage modulus and the exponent m is close to 0.5. A

similar form of the master flow characteristics was proposed by Seth et al. (2011). They used a nondimensional shear rate, $\tilde{\dot{\gamma}} = \dot{\gamma}\,\eta_s/E^*$, as the ratio of viscous to elastic forces:

$$\frac{\tau}{\tau_y} = 1 + K\left(\frac{\eta_s\dot{\gamma}}{\gamma_y^2 E^*}\right)^{1/2} \tag{3-6}$$

with the yield strain, $\gamma_y = \tau_y/G_0$, ranging from 0.02 to 0.04. The elastic modulus, E^*, is related to the particle Young modulus, E, via the Poisson ratio, ν, which for the volume conserving strain takes the value of 0.5.

$$E^* = \frac{E}{2(1-\nu^2)} \tag{3-7}$$

The micromechanical model was expanded to a three-dimensional form (Seth et al. 2011) for flow of soft glasses, where in addition to the repulsive expression the particle slippage term was included (Seth et al. 2011). The authors declare no adjustable parameters were used in the modeling but the low shear modulus G_0 was determined rheometrically (Seth et al. 2006). The experimental and validated modeling data conformed closely to the constitutive equation (3-5) with the m exponent value of 0.50 ± 0.02 (Nordstrom et al. 2010b). Flows of soft particle glasses near solid surfaces of different chemistry and roughness were the subject of a further investigation by Seth et al. (2012). It was found that in the vicinity of solid repulsive surfaces, both smooth and rough, yielding was uniform and the bulk properties were recovered, contrary to smooth attractive surfaces where two slip mechanisms were identified. Nevertheless, roughened surfaces restrained the slip of microgels.

A macroscopic model enabling to calculate the Young modulus from the centrifugal compression of arbitrary microgel suspension was published (Nordstrom et al. 2010b). The model is based on the balances of particle mass and force for spherical particles that are assumed elastic and incompressible. The maximum strain for such particles, γ_m, beyond which the material cannot be compressed, equals 0.36. For the unidirectional stress τ, the Young modulus, E, is a function of the applied strain, γ, in the proportionality:

$$E \sim \frac{\sigma[1 - (\gamma/\gamma_m)^{3/2}]}{\gamma^{3/2}} \tag{3-8}$$

Denton and Tang (2016) proposed to link elasticity theory of microgels with a new statistical mechanics theorem in a theoretical model for the internal osmotic pressure and microgel swelling.

3.4 Polyelectrolyte models

On the way to quantitatively describe mechanical characteristics of polyelectrolyte chains, it was proposed to analyze them as a chain of similar segments (blobs) (De Gennes et al. 1976). That concept was further developed (Khokhlov and Khachaturian 1982; Lifshitz et al. 1978). It was later completed by Rubinstein et al. (1994, 1996) who defined the length scale of the electrostatic blob below which the polymer-solvent interactions dominate over electrostatic repulsion. The authors presented a scaling theory for the shear modulus, G, which depends on the strand length between cross-links and on the monomer concentration, c_m. The scaling rule achieved for semi-dilute polyelectrolyte microgels without added salt reads:

$$G \sim c_m^{2/9} \tag{3-9}$$

and with a high salt concentration, c_s:

$$G \sim c_m^{7/12} c_s^{1/4} \tag{3-10}$$

The two proportions (3-9 and 3-10) were positively verified by Rubinstein et al. (1996). However, the scaling rules were found to be different when the total polymer concentration, c, was used in other experimental studies for jammed microgels (Bhattacharjee et al. 2018). Stronger scaling ($G' \sim c^{9/4}$) was obtained at low concentrations of Carbopol 980 and Ultrez 10, up to that of jamming, and a weaker scaling ($G' \sim c^1$) was found at higher Carbopol concentrations. The ETD 2020 Carbopol scaled weakly ($G' \sim c^1$) in the whole analyzed concentration range.

A path to modeling the microgel yielding was recently explored (Bhattacharjee et al. 2018). The authors analyzed the critical strain, γ_y, being a ratio of the yield stress, τ_y, to the elastic shear modulus, G'.

$$\tau_y = \gamma_y G' \tag{3-11}$$

The traditional concept of the yield-stress criterion can be replaced by a new criterion of the micro-structural parameter, which assumes a critical value when the microgel microstructure is completely destroyed (Liu et al. 2016). Based on experimental data, the critical stress value was found close to $\gamma_y = 0.13$ for five microgel types (Bhattacharjee et al. 2018). The corresponding stress correlated very well with the yield stress measured from unidirectional shear and correlated with the Herschel-Bulkley-type equation (3-12) for shear stress, τ.

$$\tau = \tau_y\left[1 + \left(\dot{\gamma}\Big/\dot{\gamma}_c\right)^n\right] \tag{3-12}$$

The $\dot{\gamma}_c$ value indicates the cross-over shear rate at which the microgels transitioned between the solid and liquid behavior (Bhattacharjee et al. 2018). The authors experimentally determined the τ_y and $\dot{\gamma}_c$ values for several Carbopol microgels of different concentrations and confirmed validity of Eq. (3-12). Meeker et al. (2004a) obtained a constant yield strain, γ_y, close to 0.06 for the microgels tested. In a study on methacrylate-type microgels, the γ_y and n values of 0.05 and 0.45, respectively, were found (Cloitre et al. 2003a). The yield strain, ranging from 0.02 to 0.04 was found in another study (Seth et al. 2011) and the value of 0.04 was also found for other yield-stress materials (Chen and Zukoski 1990). The range of published yield strains, from 0.02 to 0.13, seems to be not universal and perhaps both material-type and its concentration depending.

Microgel structural properties were also predicted by means of molecular dynamics methods, although without experimental validation (Hedrick et al. 2015). Further development of the spherical cell model was published by Denton and Tang (2016) who derived a statistical mechanics theorem to describe the effect of counterion distribution on the osmotic pressure. The Poisson-Boltzmann theory was also applied to determine the osmotic pressure from the electrostatic grand potential (Denton and Tang 2016). The molecular dynamics simulations allowed to determine thermodynamic quantities such as the osmotic pressure and the equilibrium swelling ratio and results favorably compared with experiment. Nevertheless, Muthukumar (2017) in his comprehensive review concludes there is still a long way to go to reach fully quantitative predictions for polyelectrolyte systems.

3.5 General remarks

Microgels represent one of a several types of soft condensed matter (Bonn et al. 2017), which depending on the environment conditions, behaves either as a solid or a fluid phase. Carbopol microgels contain repulsive polyion particles both below and mainly above 1 μm in size. The rich collection of published physical investigations on the nature of the yield-stress materials, both theoretical and experimental, has provided a deep understanding of mesoscale phenomena, which also occur in the process equipment. Two main mechanisms responsible for the appearance of the yield stress in amorphous materials have been identified, namely either an insufficient level of thermal fluctuations that are responsible for the glass-type transition or microstructure crowding that prevails in particle jamming transition. The presented physical descriptions have been based on theoretical models of probabilistic, mechanical or electrostatic nature. Different types of constitutive equations, including rheological ones, have been obtained from the models.

The interplay between thermal fluctuations and steric constraints of soft particles have been used in the development of advanced jamming models. Two main types of micromechanical modeling have been applied; the mechanics of population of soft deformable particles suspended in a solvent or a statistical mechanics approach that considers energetic relationships within the particle network. On the other hand, the polyelectrolyte models have been based on the Poisson-Boltzmann theory of electrostatic potential along with electrostatic interactions between macroions. Those models have been incorporated in molecular dynamics simulations and yielded results well compatible with experiments. Numerical predictions by means of all the physical models have usually been complemented with rheological and/or local velocity measurements to validate the modeling (e.g., Dinkgreve et al. 2015; Ikeda et al. 2012, 2013; Meeker et al. 2004a; Nordstrom et al. 2010a).

A range of useful quantitative relationships have resulted from the physical models and also allowed to define universal scaling rules for rheological data. The rules are applicable to yield-stress materials both to the jammed and glassy-type. The physical modeling methods have resulted in proposals of universal, nondimensional flow characteristics of microgels, Eq. (3-5), which can be applied in physical characterization of Carbopol microgels. At a stress below the yield stress, soft materials remain solid but they may occasionally undergo long-time irreversible deformations. In the majority of relevant publications, Carbopol microgels have usually been identified as simple, i.e., nonthixotropic, yield-stress materials. However, transient shear-banding was found for Carbopol ETD 2050 and steady-state banding occurs only in thixotropic materials (Divoux et al. 2010; Divoux et al. 2012; Ovarlez et al. 2009). The banding is typical of aging in glassy materials and a preshearing at sufficiently large shear rate (rejuvenation) and controlled resting was therefore suggested prior to systematic rheological measurements for Carbopol (Coussot et al. 2006).

4 Rheological characteristics of Carbopol microgels

Stress-strain attributes of Carbopol microgels are described in the following Section. It begins with a description of published yield-stress data followed by wall slip effects as

well as both steady-state and nonstationary measurement results along with relevant models.

4.1 Carbopol as yield-stress material

One of the earliest papers on rheological studies was published by Bingham (1916). The first researchers who published regular investigations on the rheology of Carbopol microgels were probably Fischer et al. (1961). Perhaps the initial comparison of the measurement methods for determining yield stress was presented by Yoshimura et al. (1987). They concluded that the three rheometric geometries: concentric cylinders, parallel plates and vane gave comparable results. A recent review presents a careful assessment of various ways of measuring yield stresses by applying steady shear, oscillatory, stress growth and creep experiments (Dinkgreve et al. 2016). The authors found the applied methods resulted in different values of yield strain and stress for both thixotropic and nonthixotropic samples. Similarly, authors of another study on nonthixotropic Carbopol microgels concluded that consistent values of the yield-stress can be obtained from i) the transition of the plot of total stress versus strain in oscillatory shear, ii) extrapolation of the flow curve and iii) from startup experiments (Dinkgreve et al. 2017). Experimental techniques to measure yield stress with probing both the liquid-to solid and solid-to-liquid transitions were discussed by Bonn et al. (2017). Residual stresses after flow cessation did not provide good estimates of the dynamic yield stress. Experimental determination of the static yield stress in S → L transition in the start-up indicated stress overshoot and the stress maximum was adopted as the static yield stress (Bonn et al. 2017; Divoux et al. 2011b). Moreover, creep experiments were also regarded as a good way to determine the static yield stress (Bonn et al. 2017). On the other hand, the character of yielding in oscillatory experiments has not been fully understood to date (Bonn et al. 2017).

In a later research, different definitions and measurement methods of yield stress were examined (Joshi and Petekidis 2018). It was decided there is no clear criterion to favor accuracy of any published definition since all they provide essential information referring to specific yielding conditions. One should notice that also indirect, computational estimates of the yield stress are in practical use. The estimates result from correlating flow curves and fitting experimental results to templates such as the Herschel-Bulkley model. However, it does not necessarily imply such a material has a real yield stress (Mewis and Wagner 2012). Based on the cited references, it seems the most accurate way of determining the dynamic yield stress is from the flow curve and the static yield stress from the creep experiment.

Concentration of Carbopol in neutralized microgels has the strongest impact on their yield stress. A quantitative relationship of the dynamic yield stress vs. concentration, $\tau_y = f(c)$, was proposed by (Piau 2007). The author correlated yield stress values for Carbopol 940 against its weight percent concentration, C. Two regimes were distinguished relative to C:

$$\tau_y = \left(\frac{C}{0.0335} - 1\right)^3 \text{ for } 0.045\,\% < C < 0.155\%, \quad \text{and} \quad (4\text{-}1)$$

$$\tau_y = 45\left(\frac{C}{0.124}\right)^{1/3} \text{ for } 0.155\,\% < C < 4.0\,\%. \quad (4\text{-}2)$$

Additional information about the influence of Carbopol concentration on the microgel yield stress can be found in a graph for ETD2050 type (Lee et al. 2011) or in a table for two concentrations of the 940 brand (Shafiei et al. 2018). It was concluded in a review paper that for a nonthixotropic yield stress material the static and the dynamic yield stresses are certainly the same and are different only for thixotropic yield stress materials (Coussot 2014). However nearly all yield stress fluids are thixotropic to some extent since the two effects are of the same origin – the interplay between the fluid microstructure and its deformation in flow (Bonn and Denn 2009; Liu et al. 2016; Mewis and Wagner 2009; Moller et al. 2006). The traditional concept of the yield-stress criterion can be replaced by a new criterion of the micro-structural parameter, which assumes a critical value when the microgel microstructure is completely destroyed (Liu et al. 2016). Microgels exhibit long-time memory of the mechanical deformation mainly close to and below the threshold stress (Cloitre et al. 2000), therefore, precise control of the deformation history is vital in rheological studies. It was found that the transition from the solid to the fully-yielded liquid occurs in Carbopol 980 microgels within an intermediate solid–fluid coexistence regime, both in a rheometer and in pipe flow (Poumaere et al. 2014). Furthermore, the existence of residual stresses stored in yield-stress materials at rest was confirmed and the residual stresses in a Carbopol microgel were estimated at about 20% of the yield stress (Lidon et al. 2017). Moreover, relaxing the residual stresses can lead to microgel deformation opposite to that in preshear.

Carbopol microgels were classified by several researchers as nonthixotropic (simple) yield-stress materials

(Bonn et al. 2017; Coussot et al. 2009; Curran et al. 2002; Hassan et al. 2015; Moller et al. 2009a; Ortega-Avila et al. 2016; Ovarlez et al. 2013; Piau 2007). A convincing argument for the simple yield-stress option was presented by Moller et al. (2009b), which was based on creep tests of 0.2% Carbopol Ultrez 10 (Moller et al. 2009a), shown in Figure 6.

For stresses beyond the yield value of 30 Pa the apparent viscosity did not depend on the stress duration time, t, but for lower stresses the apparent viscosity increased with time. This indicates that in the liquid-like state the microgel did not age (nonthixotropic liquid) whereas the solid-like microgel slowly rearranged its structure. The rearrangement resulted in increasing in time the apparent viscosity or rather decreasing shear rate at a constant shear stress.

However, while gently stirred microgels of Carbopol Ultrez 10 did not reveal thixotropy (Dinkgreve et al. 2017), slightly thixotropic behavior was found for long and strongly stirred microgels of that Carbopol (Dinkgreve et al. 2018a). In addition, mild thixotropic behavior was confirmed for a Carbopol-based hair microgel (Coussot et al. 2006). Modest thixotropy was also found for Carbopol 980 NF, just above the yield stress (Varges et al. 2019). It follows from the cited examples that the extent of thixotropy depends not only on the Carbopol type but also on the preparation protocol of the microgel, in particular on the dispersion degree of microgel particles.

Thompson et al. (2018) emphasized that the yield stress, despite treating it generally as a scalar in 1D rheological flows, has a typical 3D tensor nature. It implies that the analyzed material at the yielding point cannot be free of normal stresses even in rheometric 1D flows and this aspect has been largely omitted in the subject literature. Even the elastic response to deformation of particles in physical models and also frequently published high elastic modulus

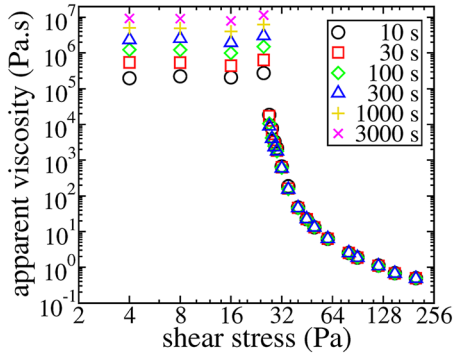

Figure 6: Apparent viscosity of Carbopol gel measured at different time, t, of stress application.
(Copied by permission from EPL 87 (2009), (Moller et al. 2009a), Figure 2a).

values, $G' > G''$, in the stress amplitude sweep tests before yielding have not drawn clear attention to normal stresses in rheological microgel characteristics. Four exceptions were found for Carbopol microgels (de Cagny et al. 2019; Piau 2007; Taylor and Gordon 1982; Thompson et al. 2018). In addition, extensive measurements of the normal force of confined Carbopol 981 particle were carried out (Jofore et al. 2015). In the Piau's work (2007), a correlation of experimental data of the first normal stress difference, N_1, vs. shear rate was proposed in the form of Eq. (4-8).

The main rheological equations of simple (nonthixotropic) yield-stress fluids can be presented in the following equations of the classical fluid mechanics written for the (i, j) components of the stress tensor, τ_{ij}, separately for the stresses above and below the yield stress, τ_y (Frigaard 2019).

$$\tau_{ij} = \left[\mu(\dot{\gamma}) + \frac{\tau_y}{\dot{\gamma}}\right]\dot{\gamma}_{ij} \quad \text{for} \quad \tau > \tau_y \tag{4-3}$$

$$\dot{\gamma} = 0 \quad \text{for} \quad \tau \le \tau_y \tag{4-4}$$

The strain rate tensor components for the fluid velocity vector, $\boldsymbol{u}$, are

$$\dot{\gamma}_{ij} = \frac{\partial u_i}{\partial x_j} + \frac{\partial u_j}{\partial x_i} \tag{4-5}$$

with the magnitude of the shear rate and stress:

$$\dot{\gamma} = |\dot{\boldsymbol{\gamma}}| = \left[\frac{1}{2}\sum_{i,j=1}^{3}\left(\dot{\gamma}_{ij}\right)^2\right]^{1/2}, \quad \tau = |\boldsymbol{\tau}| = \left[\frac{1}{2}\sum_{i,j=1}^{3}\left(\tau_{ij}\right)^2\right]^{1/2} \tag{4-6}$$

The deviatoric stress tensor, $\boldsymbol{\tau}$, i.e., the tensor left after subtracting the hydrostatic tensor, can be presented for a viscometric 1D flow as (Thompson et al. 2018):

$$\boldsymbol{\tau} = \begin{bmatrix} \frac{1}{3}(2N_1 + N_2) & \tau_{21} & 0 \\ \tau_{21} & -\frac{1}{3}(N_1 - N_2) & 0 \\ 0 & 0 & -\frac{1}{3}(N_1 + 2N_2) \end{bmatrix}, \tag{4-7}$$

where the normal stress differences are $N_1 \equiv \tau_{11} - \tau_{22}$, $N_2 \equiv \tau_{22} - \tau_{33}$, x_1 denotes the flow direction, x_2 is the direction of the velocity gradient and x_3 stands for the neutral (vorticity) direction. The dependence of the first stress difference, N_1, on the shear rate was described for Carbopol 940 in a similar formula to the H-B equation (Piau 2007):

$$N_1 = N_{1,0} + k_1\dot{\gamma}^n \tag{4-8}$$

The author emphasized that after squeezing a sample by the measuring plate or cone the internal stresses remain

in the plastic material, especially the normal stresses remain high (Piau 2007). In multidirectional (2D or 3D) deformation of plastic materials, yielding begins when the equivalent von Mises stress, τ_{vM}, reaches the yield strength, i.e., τ_y. In shear flows, the von Mises stress for the yielding point (subscript "y") should be evaluated as (Thompson et al. 2018):

$$\tau_{vM,y} = \sqrt{\tau_{21,y}^2 + \frac{1}{3}\left(N_{1,y}^2 + N_{1,y}N_{2,y} + N_{2,y}^2\right)} \qquad (4\text{-}9)$$

In order to avoid terminology ambiguity, it was proposed to label the von Mises yield stress as the true yield stress to distinguish it from the 1D yield shear stress, τ_y, generally regarded as the yield stress (Habibi et al. 2016). Thus, in the thermodynamic equilibrium a sheared material remains unyielded when $\tau_{vM} < \tau_{vM,y}$, and is yielded when $\tau_{vM} > \tau_{vM,y}$.

Two neutralized Carbopol microgels of different concentration along with three hair gels and three other commercial pastes were used in the combined rheological measurements (Thompson et al. 2018); creep tests to measure the yield stress component, $\tau_{21,y}$, and stress ramp tests to measure and evaluate the stress differences, $N_{1,y}$ and $N_{1,y} - N_{2,y}$ corresponding to $\tau_{21} = \tau_{21,y}$. The authors (Thompson et al. 2018) emphasize that all the components of the deviatoric stress tensor, $\boldsymbol{\tau}$ (Eq. 4-7), can significantly contribute to the yield criterion and this calls for reliable measurements of tensor components. Therefore, the concept of ideal viscoplastic material with the absence of elasticity is regarded as clearly inappropriate (Thompson et al. 2018).

The central issues considered in the rheological part of this review are focused on the steady-state rotational, oscillatory and transient characteristics of Carbopol microgels. However, because of the significance of the wall slip problems, presentation of the characteristics should be preceded by a description of the slip that can appear in many types of shear measurements.

4.2 Wall slip

Many soft, dispersed materials exhibit slip onto surfaces of industrial processing equipment (Cloitre and Bonnecaze 2017). In addition, the wall slip can appear both in the fluid and solid state of the material bulk (Malkin et al. 2017). Interactions between particles and particle-surface can also influence the slip (Seth et al. 2008). For particles attractive to the smooth wall a finite sliding yield stress exists below which the wall slip stops (Christel et al. 2012; Seth et al. 2008; Seth et al. 2012). That adhesion (sliding) yield stress, τ_a, is usually much smaller than the yield stress and the material slip is entirely eliminated for shear stress below the particle-wall adhesion stress (Bonnecaze and Cloitre 2010). Two dominant mechanisms of wall slip were identified, namely i) fluid–solid wall interaction and ii) shear induced solid-fluid transition (Malkin and Patlazhan 2018). Wall slip enables relaxation of excess elastic energy, which happens mostly by shear band formation (Cloitre and Bonnecaze 2017). A thorough review of microscopic techniques for investigating wall slip was presented by Cloitre and Bonnecaze (2017). The authors concluded that wall slip is a complex and fundamental component of deformation and flow of yield stress materials. A systematic review of phenomena accompanying the wall slip in complex fluids, including microgels, was recently presented (Malkin and Patlazhan 2018). The authors concluded that in viscoplastic media true slip occurs at low stresses below yield point and beyond it and apparent slip can also happen due to formation of a thin layer of low-viscous fluid at the wall.

In rheometry, the slip results in lowering the apparent viscosity and wall slip can also be present in oscillatory measurements (Yoshimura and Prud'homme 1988). A simple method of correcting for the wall slip in Couette rheometers was proposed (Kiljański 1989). The proposal was based on flow curves obtained for different rotor-stator gaps. Further corrections were published for capillary and torsional flows of viscoplastic hydrogels (Aktas et al. 2014) as well as an advanced, general approach for the parallel disk geometry (Leong et al. 2008). A typical technique of suppressing the slip is the application of corrugated shearing surfaces (Ahonguio et al. 2016a; Coussot et al. 2002; Divoux et al. 2012; Magnin and Piau 1990; Meeker et al. 2004a, 2004b).

Calculation of the shear rate of a material sample with wall slip if based on the assumption of material uniform deformation, leads to an apparent (biased) value, $\dot{\gamma}_a = V_{\text{wall}}/h$, which is more than the true rate, $\dot{\gamma}$ (Malkin and Patlazhan 2018).

$$\dot{\gamma} = \dot{\gamma}_a - \xi V_s/h \qquad (4\text{-}10)$$

The difference of the two shear rates depends on the wall slip velocity, V_s, the gap distance between two walls, h, and the number of smooth walls, ξ (1 or 2). Three slip regimes for the yield-stress materials were identified (Meeker et al. 2004b):

- Fluid regime I for the stress $\tau \geq 1.5\tau_y$ where wall slip is almost insignificant and the rheology does not depend on the wall roughness,
- Mixed regime II for $\tau_y < \tau < 1.5\tau_y$ where both slip and bulk flow become significant to the macrorheology,
- Motion of solid phase in regime III entirely due to the wall slip with $\tau \leq \tau_y$.

Magnin and Piau (1990) found significant wall slip of the studied microgel and indicated two stress plateaus of the solid material: one for the smooth and the other for corrugated cone-plate rheometer surfaces. Wall slip in two-phase materials, such as Carbopol microgels, occurs due to particles being displaced from solid surfaces by steric, hydrodynamic, viscoelastic and chemical forces (Barnes and Walters 1985). The boundary layer is therefore richer in the solvent of lower viscosity (Kalyon 2005) and the slippage is related to boundary roughness (Barnes 1995). Later on, significant wall slip of Carbopol 940 and 980 containing microgels was proved (Bertola et al. 2003; Piau 2007). It was confirmed that rheometric surface roughness has a major effect on the friction stress at low slip velocities (Piau 2007). Since the size of Carbopol particles may reach tens of micrometers, particles can slip along the surface if the size of surface corrugation is smaller than the particle size (Cloitre and Bonnecaze 2017; Jofore et al. 2015). It was also found the optimum roughness height to suppress the wall slip was close to the particle size when particles were well dispersed (Cloitre and Bonnecaze 2017). Based on controlled stress measurements with serrated plate-plate geometry for a Carbopol 940 microgel, three deformation regimes of the microgel were defined, namely elastic solid (S), power-law fluid flow (F) and an intermediate solid and fluid ($S + F$) deformation (Putz and Burghelea 2009). The regimes correspond respectively to those III, I, II proposed by Meeker et al. (2004b). Recently, further experimental evidence was published on the transition in slip regimes (Pemeja et al. 2019). A model that assumed total wall friction to be a sum of elastohydrodynamic and Stokes frictions was successfully used to explain experimental data for the wall slip of a range of Carbopol microgels (Pemeja et al. 2019). The novel approach allows to directly link wall friction with physical properties of particles and solvent.

4.3 Steady-state rotational measurements

The first rheological studies, published for Carbopol in the 1960s and 1970s, were associated with drilling fluids or pharmaceutical applications (Fischer et al. 1961; Taylor and Bagley 1974, 1975; Testa and Etter 1973). Those investigations were followed by similar basic studies (Barry and Meyer 1979a; Berney and Deasy 1979; Dolz et al. 1998; Hernandez et al. 1998). A broader approach for concentrated Carbopol 941 microgels, including yield stress analysis, was applied in 1988 by Ketz et al. (1988). They found a critical strain of 40% irrespective of concentration. An advanced study of flow curves of Carbopol 940 microgels was also published in 1990 with correlations of τ and N_1 of the H-B type and determination of the n exponent values of 0.37 and 0.39, respectively (Magnin and Piau 1990).

In order to obtain true flow curves, roughened measuring surfaces should be used to avoid wall slip of Carbopol microgels (Ahonguio et al. 2016a; Coussot et al. 2002; Magnin and Piau 1990; Meeker et al. 2004a, 2004b). For such materials sheared between roughened rheometer surfaces, the relationship of shear stress, τ, vs. shear rate, $\dot{\gamma}$, can be best represented for a wide range of shear rate in the form of the Herschel-Bulkley Equation (1-2) for measurements leading to the dynamic yield stress, τ_y (Dinkgreve et al. 2016). Yet in the plate-plate and Couette-type rheometers care should be taken for the shear rate varying inside the measured volume, which is particularly important close to the yielding range. Since below the yield stress the materials are intrinsically out of equilibrium their measurements are not reproducible unless the material mechanical history is controlled (Cloitre et al. 2003b). Therefore, some authors lay clear emphasis on the application of material preshearing with suitable shear rate to ensure repeatable results (Coussot et al. 2006; Divoux et al. 2011b; Lidon et al. 2017; Mohan et al. 2013). In order to erase the memory of structuration and use a relaxed material, rheological measurements should be done in progressively decreasing shear rate without resting (Ovarlez et al. 2013). This is valid as long as the material is liquid-like and the steady-state of shearing is then reached in a few seconds. Close to and within Carbopol microgel yielding, shear rate at constant stress evolves in relatively long time (Magnin and Piau 1990). It was found that the Carbopol 934 microgel was sheared 10^4 s before the equilibrium of stress vs. shear rate was obtained for the smallest rates below 10^{-4} s^{-1} (Shafiei et al. 2017). Comparably long testing time, of 2–5 reciprocals of shear rate, was applied by Coussot (2009). By applying proper steady-state conditions for shear stress vs. shear rate, the ramp-up and ramp-down flow curves coincide (Coussot et al. 2009; Piau 2007). A good illustration of steady-state flow curves down to very low shear rates for Carbopol 934 microgels of different concentration and pH = 4.5 is shown in Figure 7(a) (Shafiei et al. 2017) and in Figure 7(b) for 2% Carbopol 940 microgels of different pH values (Shafiei et al. 2018).

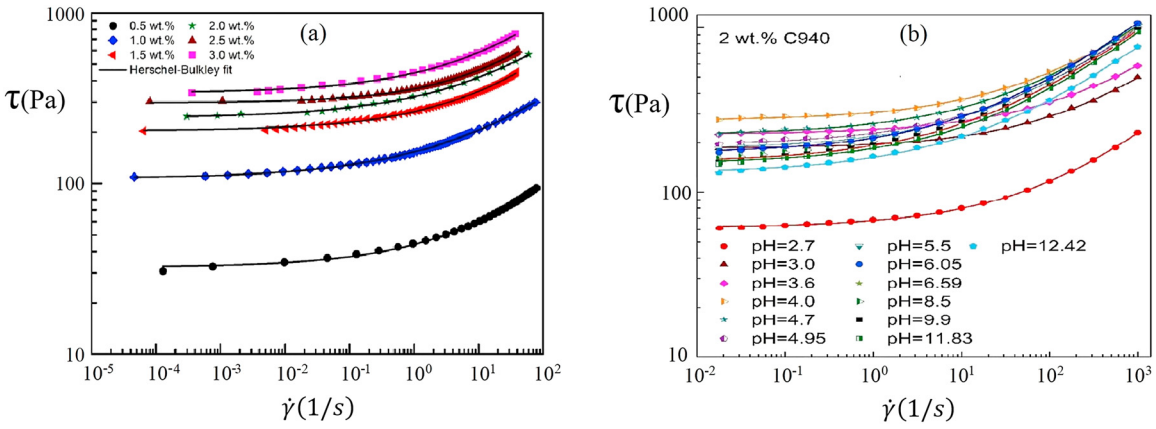

Figure 7: Shear stress as a function of shear rate for different Carbopol 934 concentrations (a) (Shafiei et al. 2017), and (b) for different pH of 2% Carbopol 940 gel (Shafiei et al. 2018). Copied by permission from Editor of Applied Rheology for Figure 2 of paper 27 (2017) 64433 and from Copyright Clearance Center's RightsLink® for Figure 3b of Polymer 139 (2018) 44-51.

The yield-stress materials, such as Carbopol microgels, may exhibit a characteristic stress vs. strain plateau of a slight slope that clearly separates the solid-like and liquid-like behavior (Uhlherr et al. 2005). The authors suggest the plateau slope depends on the material uniformity in the microscale. The microgels undergo aging at relatively slow rates and repeatable results can only be achieved if the microgels are properly rejuvenated by preshearing (Coussot et al. 2006; Divoux et al. 2011b; Lidon et al. 2017; Mohan et al. 2013). The key studies on Carbopol characterization, which were published after 2000 are presented along with a collection of the H-B parameters in Table 1.

It follows from Table 1 that the most popular Carbopol type used in rheological studies was Carbopol 940, while ETD2050 and Ultrez 10 were used less frequently. The applied Carbopol dispersions in water had weight concentrations ranging typically from 0.1 to 5% and they were usually neutralized with NaOH and seldom with triethanolamine. The strongest effect on the Carbopol microgel rheology is exerted by its concentration (Barry and Meyer 1974; Di Giuseppe et al. 2015; Dinkgreve et al. 2016; Gutowski et al. 2012; Hassan et al. 2015; Jofore et al. 2015; Piau 2007; Roberts and Barnes 2001; Shafiei et al. 2018; Shafiei et al. 2017; Weber et al. 2012). Higher concentrations of several Carbopol microgels result in their higher yield stress (Di Giuseppe et al. 2015; Dinkgreve et al. 2016; Gutowski et al. 2012; Roberts and Barnes 2001; Varges et al. 2019; Weber et al. 2012). Moreover, higher yield stress of Carbopol 980 microgels led to moderate increasing their shear thinning capability by lowering the flow index, n, of the H-B equation, e.g., from 0.6 to 0.3 (Di Giuseppe et al. 2015; Roberts and Barnes 2001; Weber et al. 2012) or in a little wider range of n depending on the concentration of Carbopol Ultrez 10 (Gutowski et al. 2012) or Ultrez 20 (Hassan et al. 2015). Analogous trends were found with lower exponents for Carbopol 980 NF (Islam et al. 2004) and Carbopol Ultrez 10 (Jimenez et al. 2007) neutralized with triethanolamine. Joint effects of the concentration (0.5–3 wt.%) and pH (3–12) on the H-B parameters of Carbopol 934 and 940 microgels were also reported in two recent papers (Shafiei et al. 2018; Shafiei et al. 2017). Again, the yield stress and consistency index values were growing with increasing concentration. However, the flow index for Carbopol 940 was found close to 0.45 irrespective of pH for the 2% microgel but for the 3% concentration it displayed a flat maximum close to $n = 0.7$ at pH of about 7.

Regarding the pH influence, of Carbopol dispersions in water, it can be concluded that even slight neutralization to about pH = 4 strongly rises their yield stress, irrespective of Carbopol type. Further alkalization to about pH = 8 results in flat maxima of τ_y at about pH = 6 (Fischer et al. 1961; Islam et al. 2004; Lee et al. 2011), while additional rise in pH causes first slow decrease followed by strong reduction of τ_y from pH about 11 onwards (Gutowski et al. 2012). Generally, the n index of the H-B equation changed rather little with increasing pH and initially decreased from about 0.8 for non-neutralized suspension and then reached flat minima of about $n = 0.4$ at pH from 6 to 7. Examples of recent experimental studies on the influence of pH and concentration of Carbopol 934 and 940 microgels on estimated values of parameters of the H-B equation, Eq. (3-5), for the yield stress and flow index are shown in Figure 8(a) and (b) (Shafiei et al. 2018; Shafiei et al. 2017).

The results shown in Figure 8 are generally in line with the remarks in two previous paragraphs, except for the flow index for highest concentration of Carbopol 940. It has also been well confirmed the flow curves for Carbopol microgels appear relatively insensitive to temperature (Barry and

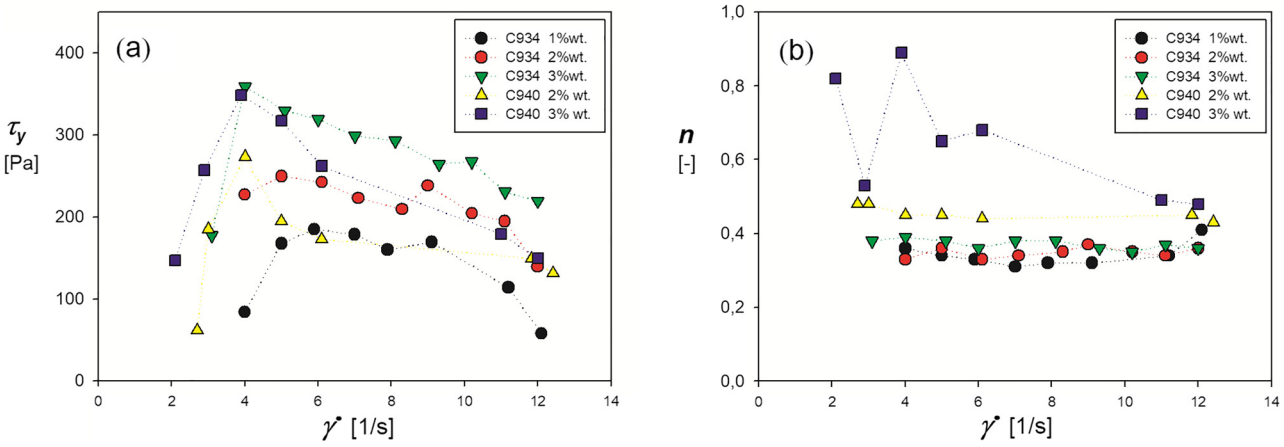

Figure 8: Effects of pH and concentration of Carbopol 934 (Shafiei et al. 2017) and 940 gels (Shafiei et al. 2018) on yield stress (a) and flow index (b).

Meyer 1974; Fischer et al. 1961; Gutowski et al. 2012; Hassan et al. 2015; Islam et al. 2004; Peixinho et al. 2008).

Validity of the nondimensional form (3-5) of the Herschel-Bulkley relationship, presented graphically in Figure 9, was confirmed for Carbopol 934 microgels (Shafiei et al. 2017).

Modeling of soft matter mechanics yielded the exponent m = 0.45 (Bonnecaze and Cloitre 2010; Cloitre et al. 2003a), whereas a similar model led to m = 0.5 in Eq. (3-5) (Seth et al. 2011). Other generalizations of the flow curve relationship were also proposed, which were based on the distance to the jamming point (Dekker et al. 2018; Dinkgreve et al. 2015). Nevertheless, universality of the (3-5) relationship for different Carbopol types, concentrations and pH still needs to be confirmed.

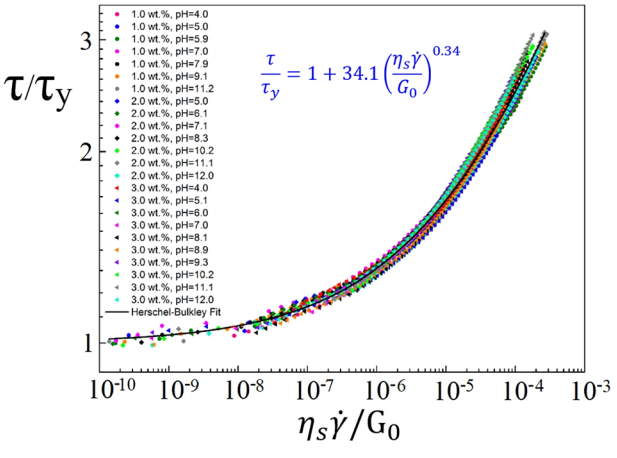

Figure 9: Universal, nondimensional correlation of shear stress versus shear rate (Shafiei et al. 2017). Copied by permission from Editor of Applied Rheology 27 (2017) 64433, Figure 7.

4.4 Sinusoidal oscillation measurements

The most popular nonsteady-state tests have consisted in regular oscillatory measurements. The dynamics of small amplitude (linear) oscillatory shearing (SAOS) and the large amplitude oscillatory shearing (LAOS) was initially analyzed in 1982 for negligible fluid inertia in rheometry (Macsporran and Spiers 1982a, 1982b). The first systematic oscillatory study of Carbopol 940 and 941 microgels was published by Barry and Meyer (1979b). The authors found the studied microgels, of 1–5% wt. concentration, behaved essentially as elastic bodies since $G' > G''$ and both moduli moderately raised with growing oscillation frequency. A similar prevalence of $G'>G''$ in wide ranges of varied frequency, ω, was found in several studies for different Carbopol microgels: 940 (Agarwal and Joshi 2019; Carnali and Naser 1992), 941 (Kim et al. 2003), ETD 2050 (Divoux et al. 2011b), Ultrez 10 (Gutowski et al. 2012), Ultrez 20 (Hassan et al. 2015; Varges et al. 2019). The common feature of the investigations were low values of strain, $\gamma < 10\%$, and the shear stress below yielding, $\tau < \tau_y$. In those conditions, the G' and G'' values and shear-thinning grew with increasing microgel concentration (Di Giuseppe et al. 2015; Divoux et al. 2011b; Hassan et al. 2015; Shafiei et al. 2018; Varges et al. 2019). Akin to other studies, (e.g., Agarwal and Joshi 2019; Harrington 2012; Malkin et al. 2017; Varges et al. 2019), practically constant values of G' were found at low oscillation frequencies for $\tau < \tau_y$ and this was considered characteristic of the solid state of microgels (Hassan et al. 2015), e.g., the τ = 10 Pa lines (open symbols) in Figure 10. An evolution of the relation between the two moduli was already found in an early study (Ketz et al. 1988). While for strains, γ, below

10% nearly constant G' and G'' were first obtained with $G' > G''$, then for higher strains a gradual decrease of G' and increase of G'' lines was found along with their intersections e.g., the τ = 40 and 100 Pa lines (gray and blue symbols, respectively) in Figure 10. Such an intersection of the G' and G'' curves vs. γ at a constant ω was also obtained in a range of later investigations using different Carbopol microgels. The critical strain, γ_G, for which $G' = G''$, increased with the Carbopol microgel concentration (Di Giuseppe et al. 2015; Shafiei et al. 2018). A small influence of the microgel relaxation time was observed for G'' while G' remained constant (Agarwal and Joshi 2019). The dynamic moduli of Carbopol Ultrez 20 varied insignificantly (G') or little (G'') with temperature in oscillation experiments (Hassan et al. 2015). When considering the pH effects on the dynamic moduli, it was determined for Carbopol microgels the maximum values of G' and G'' appear close to pH = 5 and their values decreased with the pH distance from 5 (Di Giuseppe et al. 2015; Shafiei et al. 2018). In a recent paper of the de Souza Mendes team, Carbopol NF 980 dispersions in water and water-glycerol were tested in oscillation measurements both in the linear SAOS and the quasilinear large-amplitude oscillatory shearing, QL-LAOS, modes (Varges et al. 2019). Such a subrange of LAOS was predicted theoretically for yield-stress materials using the model presented by Mendes and Thompson (2013). To prove that assumption the authors modeled sudden application of a constant shear rate to a fully relaxed material. At very early times after the start, of the order of one period of oscillation, the elastic stress remained below the yield stress. Consequently, within the time period no creep occurs in yield-stress materials and their microstructures remain unchanged. Furthermore, the elastic deformation increases then linearly in time. Thus, by application of sufficiently high frequency of LAOS at fixed stress amplitude, such constant-structure motion can be realized giving a sinusoidal output wave of stress and rate (Mendes et al. 2014b). This is similar to the appearance of linear viscoelastic region in the low end of strain amplitudes, and that technique is therefore called pseudolinear. A methodology simpler than that in (Mendes et al. 2014b), for determination of material properties was developed for the quasilinear flow regime, QL-LAOS (Leite et al. 2019).

An example of our own oscillatory measurements of a Carbopol Ultrez 30 microgel is shown in Figure 10. The data were obtained in a corrugated cone-plate geometry at 3 levels of constant shear stress, τ, both below the yield stress, τ_y, (open symbols) and above it (grey and blue symbols).

For low shear stresses below the microgel yield stress, $\tau < \tau_y$, the storage modulus, G', (circle icons) prevails over the loss modulus, G'', (triangle icons) irrespective of the oscillation frequency, ω, confirming the solid-like behavior

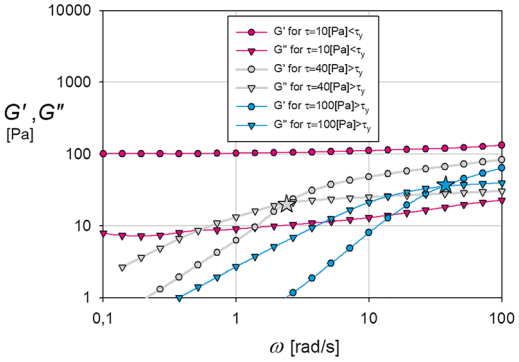

Figure 10: The storage and loss moduli, G' and G'', of 0.2% Carbopol Ultrez 30 gel against the oscillation frequency, ω, for 3 levels of constant shear stress in a rough cone-plate system.

of the microgel. With the growing frequency at constant stress levels being higher than the yield stress, first the viscous forces are higher than the elastic ones, i.e., $G'' > G'$, and the microgel behaves as a liquid. It indicates the microgel particles are responsive enough to follow oscillating deformations. Since G' grows with ω faster than G'' for $\tau > \tau_y$, then at some frequency, ω_G, the two moduli get equal. That cross-point value of $G''_c = G'_c$ (star icons) was suggested in the literature as a good estimate of the material yield stress (Metivier et al. 2017; Perge et al. 2014). However, the cross-point stresses shown by star signs in Figure 10 significantly depend on the oscillation frequency. Therefore, that cross-point stress cannot be accepted generally as a proper material property (Varges et al. 2019). For shear stresses above the yield stress and frequencies higher than the critical frequency, ω_G, the storage modulus exceeds the loss modulus, which implies the microgel cannot then freely flow and it deforms mainly elastically.

A match of the functions of: i) apparent viscosity $\eta_a = \tau/\dot{\gamma} = f(\dot{\gamma})$ for steady shearing and ii) complex viscosity, $\eta^* = (G'^2 + G''^2)^{1/2}/\omega = f(\omega)$ for oscillatory measurements was proposed for polymer materials by Cox and Merz (1958). The anticipated equality, known as the Cox-Merz rule, can be expressed as:

$$\eta_a(\dot{\gamma}) = |\eta^*(\omega)|_{\omega=\dot{\gamma}} \tag{4-11}$$

However, that rule was found invalid for microgel dispersions (Curran et al. 2002; Ketz et al. 1988) or other soft materials with yield stress (Li et al. 2005; Sollich 1998). Nevertheless, Doraiswamy et al. (1991) were perhaps the pioneers of successful extension of the rule to yield-stress materials, it is also named the Rutgers-Delaware rule (Mewis and Wagner 2012). The concept is based on the maximum value of sinusoidally varied local strain from neutral position, γ_0, and a newly defined effective

(maximum) shear rate, $\gamma_0\omega$, which is expected to replace the actual shear rate, $\dot{\gamma}$, in the Cox-Merz rule.

$$\eta_a(\dot{\gamma}) = |\eta^*(\gamma_0\omega)|_{\gamma_0\omega=\dot{\gamma}} \tag{4-12}$$

That concept was successfully validated for silicon particles in polyethylene (Doraiswamy et al. 1991). A similar proposal to the Cox-Merz rule, but for the first normal stress difference, N_1, = $f(G', G'')$ was published for polymer melts in 1986 by Laun (1986). An extension of the Cox-Merz and Laun rules onto the $N_1(\dot{\gamma})$ relationship was also proposed but it has not yet been tested for yield-stress materials (Sharma and McKinley 2012).

4.5 Elasto-viscoplastic rheological models

Relations between measurable rheological quantities in oscillatory experiments can be well reproduced by elasto-viscoplastic models. Two such advanced models were proposed (Mendes and Thompson 2013; Saramito 2009), and the models are briefly presented below.

A constitutive, thermodynamically verified, rheological model for elasto-viscoplastic (EVP) materials was developed by Saramito (2007, 2009). The first version for Bingham materials was extended to Herschel-Bulkley fluids (Saramito 2009) using the elastic stress tensor, $\boldsymbol{\tau}$, as the product of elastic modulus, G, and elastic strain tensor, $\boldsymbol{\gamma}_e$,: $\boldsymbol{\tau}$ = G $\boldsymbol{\gamma}_e$ (Saramito 2007). The elastic deformation tensor added to the plastic one, $\boldsymbol{\gamma}_p$, forms the total deformation tensor: $\boldsymbol{\gamma} = \boldsymbol{\gamma}_e + \boldsymbol{\gamma}_p$. The mechanical model is represented in the fluid mechanics notation in Figure 11.

The spring with modulus, G, characterizes elastic stress, τ, two dashpots represent viscous dissipation proportional to the total deformation rate, γ, the solid friction element of constant resistance represents plastic deformation that occurs when the elastic stress, τ, is larger than the yield stress, τ_y. The total stress, σ, is the sum of the elastic, τ, and viscous, $\eta_s\dot{\gamma}$, stresses. The constitutive 3D equation can be presented as follows (Saramito 2007, 2009; Saramito and Wachs 2017; Syrakos et al. 2020):

$$\frac{1}{G}\dot{\tau} + max\left(0, \frac{|\tau_d| - \tau_y}{k|\tau_d|^{n-1}}\right)^{1/n} \tau = \dot{\gamma} \tag{4-13}$$

where $|\tau_d|$ is the matrix norm of the deviatoric part of the stress tensor, τ_y is the yield stress scalar and k, n are constants of the Herschel-Bulkley Equation (1-2). The rates of stress and deformation are denoted by $\dot{\tau}$ and $\dot{\gamma}$, respectively. A closure of the Saramito's differential model (4-13) for predicting elasto-viscoplastic flows requires addition of two differential conservation equations for momentum and mass of the material. Understanding rheological features of the EVP materials requires simultaneous consideration of three contributions: elastic, plastic and viscous (Cheddadi et al. 2011). A comparison of results of the thermodynamically admissible EVP model (Saramito 2009) and two regularized yield-stress models against experimental data for falling of solid spheres in 0.07% Carbopol 940 (Holenberg et al. 2012) indicated superiority of the differential model (4-13) (Fraggedakis et al. 2016).

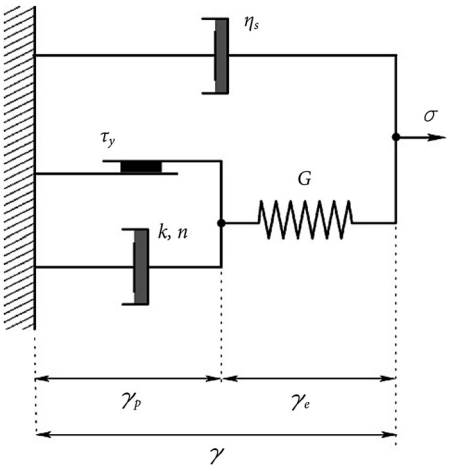

Figure 11: Scheme of the elasto-viscoplastic model (Saramito 2009).
By permission of the *Journal of Non-Newtonian Fluid Mechanics*.

Significant progress in the theory of the elasto-viscoplastic yield-stress materials and related rheometrical applications has also been made by the research group led by de Souza Mendes. It was initially proposed to enrich the Maxwell-type rheological model by allowing model parameters of thixotropic viscoelastic fluids to be dependent on the material microstructure (Mendes 2009). Two first-order differential equations constituted that rheological model; one for the shear stress and another one for the structure parameter. In the following model version, its authors Mendes and Thompson (2013) advised to vary the structure evolution parameter, λ, from zero (fully unstructured) to a large positive number (fully structured). That model version corresponds to the Jeffreys constitutive model with its material functions dependent on the structure parameter. The mechanical analog of the Jeffreys model can be obtained from the Kelvin-Voigt unit with a second dashpot added in series to the elastic element (Mendes and Thompson 2013). The following Jeffreys functions are involved in the model: the elastic modulus, G, relaxation time, θ_1, retardation time, θ_2, structural viscosity, η_s, steady-state viscosity, η, which is the sum of η_s and η_∞ (Leite et al. 2019). The Jeffreys

material functions can be determined using the steady-state and oscillatory data of η, G', G'' (Leite et al. 2019):

$$G = G'\left[1 + \frac{G'^2}{(\eta\omega - G'')^2}\right] \tag{4-14}$$

$$\theta_1 = \frac{\eta\omega - G''}{G'\omega} \tag{4-15}$$

$$\theta_2 = \frac{G''}{G'\omega} - \frac{G'^2 + G''^2}{\eta G'\omega^2} \tag{4-16}$$

$$\eta_s = \eta - \frac{G''}{\omega} + \frac{G'^2}{\eta\omega^2 - G''\omega} \tag{4-17}$$

$$\eta_\infty = \frac{G''}{\omega} - \frac{G'^2}{\eta\omega^2 - G''\omega} \tag{4-18}$$

For the hair gel used in the study, $\eta_s >> \eta_\infty$, therefore $\eta_s \cong \eta$ and, consequently, η_s was found weakly dependent on the oscillation frequency (Leite et al. 2019). The results convincingly confirm that the developed QL-LAOS analysis can offer a simple way of determination of the material properties (Leite et al. 2019), much less complex than a typical Fourier-transform approach as in (Ewoldt et al. 2008; Ewoldt et al. 2010; Hyun et al. 2011). One can conclude the two elasto-viscoplastic models offer good theoretical basis for analysis of oscillation rheometric data for Carbopol microgels.

4.6 Transient shear measurements

Creep is defined in rheology textbooks as slow deformation of material (Barnes et al. 1993), slow development of deformations (Malkin and Isayev 2006) or slow viscous flow (Mewis and Wagner 2012). Creep measurements can be carried out for structured samples in two modes: i) instantly imposed constant values of either constant stress (creep test) or shear rate (shear start-up test) or strain (strain test) or/and ii) creep recovery after the stress has been instantly removed (Macosko 1994). Nevertheless, creep test is usually conducted by applying various constant stresses to a sample, that has been at rest for sufficiently long time, and corresponding strain variations are recorded in time (Malkin and Isayev 2006; Mewis and Wagner 2012). In small strain tests, two time-dependent quantities are generally used in material characterization; the relaxation modulus, G, and creep compliance, J. The relaxation modulus, G, is defined by means of the transient shear rate, τ, divided by the initial strain, γ_0.

$$G(t) = \frac{\tau(t, \dot{\gamma})}{\gamma_0} \tag{4-19}$$

The shear stress is a function of time, t, and the shear rate, $\dot{\gamma}$. In transient measurements with plate-plate measuring systems, the correction for the shear stress at the plate rim can be found from the relationship similar to that for the steady-state (Genani and Powell 1985), but now only for the given time instant, t (Mendes et al. 2014a).

$$\tau\left(\dot{\gamma}_R, t\right) = \frac{M_{P-P}\left(\dot{\gamma}_R, t\right)}{2\pi R^3}\left\{3 + \frac{d\left[\ln M_{P-P}\left(\dot{\gamma}_R, t\right)\right]}{d\left(\ln \dot{\gamma}_R\right)}\right\}_{t=\text{fixed}} \tag{4-20}$$

Creep compliance, J, expresses the ratio of the changing strain, $\gamma(t)$, that results from an instant increase of the stress from 0 to τ_0 (Macosko 1994).

4.6.1 Start-up flows

The first creep data for Carbopol 940 and 941 were published in 1979 in the form of creep compliance graph (Barry and Meyer 1979a). The authors also estimated specific retardation times of the microgels at the level of several hundred of seconds. The retardation time is the time to reach a new equilibrium orientation of polymer macromolecule. About a decade later, a report was published on shear strain of Carbopol 941 microgel resulting from the application of two levels of constant shear stress, τ, lasting for about 1000 s (Ketz et al. 1988). In the case of $\tau < \tau_y$, an equilibrium (constant) strain was quickly obtained, which can be followed by complete recovery when stress removal occurs. On the contrary, when a stress higher than the yield stress was applied, the material deformed irreversibly and it even showed a small strain overshoot followed by a constant shear rate (Ketz et al. 1988). Stress overshoot at constant shear rates was also accomplished in other studies: with Carbopol 940 (Agarwal and Joshi 2019; Magnin and Piau 1990; Piau 2007), Carbopol 934 (Uhlherr et al. 2005), Carbopol Ultrez 10 (Dinkgreve et al. 2018a), Carbopol NF 980 (Varges et al. 2019), Carbopol-based hair microgel (Coussot et al. 2006; Mendes et al. 2014b; Moller et al. 2009a; Thompson et al. 2018) or another microgel (Cloitre et al. 2003b). The yielding threshold was characterized by a critical strain, $\gamma_y = 0.05$, comparable to such strains of other yield-stress materials (Cloitre et al. 2003b). Coussot et al. (2006) investigated the effects of aging on the strain dynamics of three yield-stress materials. The authors found for a hair gel that at a constant shear stress below a critical value of τ_e, that was significantly smaller than τ_y,

the strain first increased quadratically in time, underwent fluctuations then kept constant and finally strongly decreased. That last change was attributed to the relaxation end of internal stresses accumulated in the preshear and the initial fluctuations were linked to the material elasticity (Coussot et al. 2006). Two types of the shear rate change in time of a hair gel were applied for constant shear stress; i) steadily decreasing shear rate for stresses below τ_y in the solid microgel, or ii) the shear rate aiming at a constant value for stresses above τ_y, which is characteristic of fluids (Mendes et al. 2014b). In constant shear rate tests, the material showed changes characteristic of the solid state until the yielding level was achieved (Mendes et al. 2014b).

Lidon et al. (2017) carried out several long-term creep tests for Carbopol ETD 2050 microgels below yielding to find out the interplay between the creep and residual stresses. The cone-plate geometry was used in creep experiments with preshear followed by a rest time. For shear stresses imposed below a critical value of $\tau_c \cong 0.2\tau_y$, anomalous creep was detected with initial decrease of strain then stabilization and eventually increase. This was attributed to the existence of viscoelastic-type residual stresses of the order of τ_c. For stresses exceeding τ_c, robust power-law creep of Andrade-type was found regardless of the microgel aging. In all investigated cases, initial inertia-elastic oscillations in the strain occurred and lasted a couple of seconds.

In the quantitative analysis of the measured strain, γ, vs. time, t, the balance of instantaneous dynamic stresses in the rheometer were used (Coussot et al. 2006):

$$I\ddot{\gamma}(t) + \mu\dot{\gamma}(t) + G\gamma(t) = \tau(t) \tag{4-21}$$

where I denotes the inertia of the system, $\ddot{\gamma}$ and $\dot{\gamma}$, stand for the second and first time derivatives of the shear strain, γ, μ is the effective viscosity of the Kevin-Voigt viscoelastic model, G stands for the elastic modulus and τ is the apparent shear stress measured by the rheometer.

Our own experimental creep data of a Carbopol microgel obtained at different shear stress levels in a rough cone-plate system are shown in Figure 12.

During the first time phase, up to about 0.05 s, all $\gamma(t)$ lines grow quadratically in time, which indicates prevalence of the instrument inertia expressed by the first term in Eq. (4-21). With the exception for the highest shear stress of about 5 τ_y, the $\gamma(t)$ creep curves have oscillations up to the time of about 1 s. The oscillations were attributed to the coupling of microgel elasticity and instrument inertia (Baravian and Quemada 1998). The damped oscillatory strain response during creep experiments is called "creep ringing" (Ewoldt and McKinley 2007). The oscillation magnitude decreases with growing shear

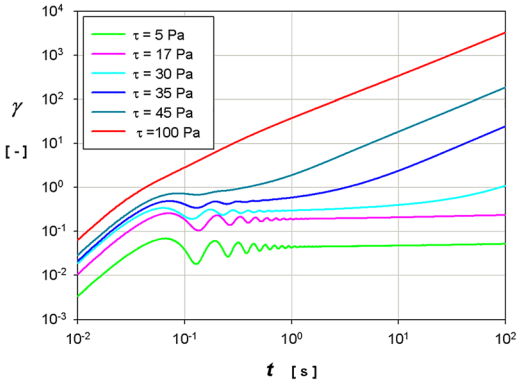

Figure 12: The start-up characteristics, γ vs. t, for six levels of constant shear stress for a 0.2% Carbopol Ultrez 30 gel of the yield stress of 19.6 Pa.

stress, cf. Figure 12. The γ creep lines in the final time range, $\tau > 1$ s, are almost horizontal with very slow growth for $\tau < \tau_y$ or grow in time for $\tau > \tau_y$, approaching the linear dependence $\gamma(t)$ due to flow of the material at constant viscosities.

A wide experimental program on stress overshoot during start-up, with imposed shear rate on Carbopol ETD 2050 microgel, was conducted in a Couette system by Divoux et al. (2011b). At small strains the microgel experienced linear increase in the shear stress then gradually slowed the growth up to reaching the maximum stress where microgel failure occurred. This was followed by a strong elastic recoil followed by a slow decrease in the shear stress towards its steady-state value. Moreover, although experiments performed for a hair gel included startup flow tests with constant shear rate, no stress overshoot was noticed for the gel (Mendes et al. 2014b). Similarly, other authors also did not find stress overshoot in Carbopol Ultrez 10 microgel samples in their startup experiments, with the exception of the hysteretic Carbopol sample which earlier experienced a long, intense stirring (Dinkgreve et al. 2016).

4.6.2 Creep recovery (shear stress relaxation)

One of the first creep recovery experiments was published in 1988 for Carbopol 941 reporting full elastic recovery of strain when the stress below yielding point was applied (Ketz et al. 1988). Furthermore, Coussot et al. (2006) confirmed that residual, irreversible deformations occurred for stresses higher than the critical stress and lower than the yield stress. In addition, microgel deformation was found to be not fully reversible after stress release (Coussot et al. 2006; Uhlherr et al. 2005), which confirms that also residual microgel deformations depend on the rest time. A closer insight into

the internal, residual stress, τ_r, of Carbopol ETD 2050 resulted from the investigations of Lidon et al. (2017). The residual stress was independent of the preshear duration and decreased with the preshear rate, $\dot{\gamma}_p$, as $\dot{\gamma}_p^{-0.2}$. The internal stress results from very slow relaxation (aging) of trapped microgel microstructure since the τ_r value roughly corresponds to the τ_c threshold stress of the Andrade power-law creep (Lidon et al. 2017). However, the internal flow characteristics require further research to better understand the complex behavior of Carbopol and other yield-stress fluids (Coussot 2014).

Moreover, Lodge and Meissner (1972) derived a new relationship of the first normal stress difference, N_1, vs. shear stress, τ, for a viscoelastic, isotropic and incompressible liquid subjected to an instantaneous shear strain, γ, at time $t = 0$.

$$N_1(t) = \gamma\tau_{21}(t) \tag{4-22}$$

The function of Eq. (4-22) was confirmed to be also valid for isotropic, perfectly elastic solids (Lodge 1975). However, validation of that relationship for Carbopol microgels has not yet been found in the analyzed literature, perhaps because of the residual stresses which are difficult to control.

One can conclude that since the strain response of Carbopol microgels in creep experiments clearly depends on the preshear rate, $\dot{\gamma}_p$, and time, t_p, and also on the waiting (relaxation) time, t_w, before measurements, therefore the three quantities should be controlled and reported for all rheological experiments with Carbopol microgels.

4.7 Comments on Carbopol rheology

The yield stress for both simple and nonsimple yield-stress fluids is recognized not to be a unique material property but its value depends also on the history of material deformation. Typically prepared Carbopol microgels have been classified as simple yield-stress fluids, practically free of thixotropy, albeit after long intensive shearing some thixotropy was found. This is probably due to the production of small microgel particles, which are prone to thermal fluctuations. Carbopol microgels can preserve residual stresses for a long time, i.e., microgels have long relaxation time of stresses, especially when the content of submicron particles is tiny. In that context, Agarwal and Joshi (2019) recently posed an open question whether Carbopol microgels belong to a constant yield-stress system that does not show any nonmonotonic flow curves.

Various rheological tests have shown the importance of the preshear procedure in assuring repeatability of Carbopol measurements. Moreover, the rheological characteristics of Carbopol microgels can be significantly affected by the wall slip, which is attributed to the formation of a submicron layer of water between the shearing walls and repulsed microgel particles. The present state of knowledge allows to quantify the wall slip effects and also effectively prevent them by applying an appropriate wall roughness. According to Cloitre and Bonnecaze (2017), open questions still remain regarding the role of wall slip in relaxing elastic stresses and its effects on velocity profiles in confined flows and in slip driven flows.

It has been experimentally verified that flow curves, τ vs. $\dot{\gamma}$, of Carbopol microgels can be well expressed by the Herschel-Bulkley equation. Effects of microgel concentration, pH and temperature on the parameters of the H-B relationship (Eq. 1-2) have been already widely tested. Also, the conditions of achieving repeatable flow curves have been convincingly explained. Using the nondimensional groups (Eq. 4-10), the convergence of individual flow curves into one master curve has been successfully achieved. Furthermore, Dinkgreve et al. (2017) succeeded in deriving coherent values of the yield stress from the steady-state flow curve and two types of transient measurements.

The dynamic moduli, G' and G'', for Carbopol microgels have been found to be weakly dependent on the oscillation frequency, ω, for a constant shear stress below the yield stress, where $G' >> G''$. Characteristic crossing of G' and G'' lines have been obtained for growing oscillations at constant shear stresses and the crossing point $G'_G = G''_G$ value was found dependent on the frequency. Two advanced constitutive models of elasto-viscoplastic fluids were successfully developed. Modifications of the Cox-Merz rule to the shear stress and the first normal stress difference of Carbopol microgels are still in the stage of testing.

Transient shear measurements, both in the start-up or flow cessation versions, have proved their usefulness in determining the properties of yield-stress materials. Stress relaxation experiments have revealed dynamics of the material microstructure and the existence of residual stresses in Carbopol. It follows from the literature review that modern rheological approaches usually comprise material analysis using two or more of those shear flows.

Due to a clear evidence of significant normal stresses in sheared Carbopol microgels, advanced rheological measurements of the microgels should also encompass normal stress components of the stress tensor. Recent investigations delivered evidence that the two normal stress differences as

well as the corresponding von Mises stress should be taken into account in designing practical applications of Carbopol microgels. This requires further, advanced research.

It should be added that the published studies on Carbopol flows have usually neglected the significance of extensional viscosity. Extensional flow characteristics of different yield-stress materials can be found elsewhere (Louvet et al. 2014; Nelson et al. 2018). A comprehensive framework for modeling elasto-viscoplastic behavior of complex fluids by means of a kinematic hardening (KH) model was recently presented (Dimitriou and McKinley 2019). The KH model accounts for the well tested complexities exhibited by Carbopol microgels, including thixotropy, nonlinear elasticity and normal stress differences. Besides, new horizons are open for experimental research of complex fluids by means of microrheology, which has recently been significantly developed (Waigh 2016). The microrheology techniques are based on the motion of introduced tracer particles, either as their passive thermal fluctuation or variations induced by external forces (Del Giudice et al. 2017).

5 Concluding remarks, outlook

The chemical contribution to presenting Carbopol microgels as model yield-stress fluids if measured with the number of cited papers, is less than either the physical or rheological input. The molecular composition of Carbopol has been well recognized as a cross-linked polymer of acrylic acid, although without precise information about the molecular scale mainly due to the confidential Carbopol grade compositions. This shortcoming may result from the requirements of specific preparation of samples for typical atomic scale instruments since a preparation usually alters microgel samples, by drying or at least by dilution in atomic force microscopy (Aufderhorst-Roberts et al. 2018). Moreover, the average size of swollen microgel particles is mostly well above 1 μm, which may suggest the particles are agglomerates of several individual Carbopol macromolecules. That hypothesis is supported by the experimental finding that intense shearing could change rheology of Carbopol microgels (Dinkgreve et al. 2018a) and this deserves further research.

In hydrated and neutralized particles, small water molecules fill the internal space between disentangled repulsive chains that contain dissociated carboxylic groups covalently bonded to every other carbon atom in the polymer chains. The molecular proportion of water to acrylic acid monomer in the typical Carbopol microgels is huge, approximately 1000 to 1. Therefore, the chemical viewpoint may be used in explaining the mechanism of shear-thinning and the very slow progress towards the equilibrium state of Carbopol hydrogels so far. Water dipoles are well known to form several clusters (Liu et al. 1996) with weak hydrogen bonds (Manogaran 2019; Montero et al. 2000). The clustering processes have slow kinetics and a low energy change of up to 30 kJ/mol (Montero et al. 2000). It is thus reasonable to assume that separation of minor portions of absorbed water from the verge of swollen Carbopol particles, along with bending of the stretched free ends of polymer chains, requires some external energy like that in microgel shearing. This reasoning leads to the hypothesis that the release of a part of absorbed water from swollen Carbopol particles to interparticle slits can be responsible for lowering internal friction between particles. With stronger shearing more water can be released and this results in lowering of the apparent microgel viscosity, which may explain the shear-thinning rheology of Carbopol microgels. It should be added here that shape deformation of Carbopol microgel particles at shearing was already predicted (Bhattacharjee et al. 2018).

In addition, the postulate of water clustering after relocation to less or no-sheared hydrogels can be supported by very slow growth in strain, as shown in Figure 12 for shear stresses below the yield stress and times longer than 1 s. It may be interpreted as a several-hour process of restoring the fully relaxed, equilibrium microgel structure along with forming water clusters in Carbopol particles. To verify the hypothesis, advanced micro- and nanoscale observations in shearing microgels are proposed as a future direction of chemical characterization.

A further direction of investigations of Carbopol microgels is searching for distribution of the cross-link density, which may be expected to decrease from the particle center towards its periphery, similarly to other microgels (Saunders and Vincent 1999). The chemical-type interaction between hydrogels and solid walls can bring a novel insight into the wall slip. In predicting flows of elasto-viscoplastic materials by means of Computational Fluid Dynamics, there are clear needs in the modeling for validated account of the 3D stress components, including normal stresses.

In the last decade, a further significant progress has been achieved in the physical modeling tools for hydrogels and, in particular, for Carbopol microgels. Very slow aging of Carbopol microgels was explained by relatively large size of microgel particles, which are only mildly sensitive to thermal fluctuations and therefore very slowly strive for the equilibrium state of the minimum of free energy. The key future investigations, that were suggested in the reviewed papers that focused mainly on the physical approach, can be collectively presented as: i) microscopic viewpoint on yielding dynamics, both experimental and theoretical, ii)

closer insight into confined flows of yield-stress materials (e.g., Waisbord et al. 2019; Younes et al. 2020b),), iii) use of statistical mechanical models to better explore the microstructure evolution in aging and rejuvenation of the materials, iv) exploration of the thermodynamic effects that accompany aging and rejuvenation with a help of the SGR model, v) more experimentation and model developments for charged macromolecules and structure of absorbed/released water, as suggested in the remarks on chemical characterization, vi) establishing a relation between particle morphology and physical aging/rejuvenation of Carbopol microgels.

The reviewed achievements in rheological description of Carbopol microgels are preceded by comprehensive presentation of research in yield stress and wall slip, which are critical in the rheology of Carbopol hydrogels. Wall slip can be effectively avoided by employing corrugated shearing surfaces in measuring instruments. It should be emphasized that in a rheometric characterization of Carbopol microgels the history of material deformation is of profound importance. Therefore, application of a controlled preshear is firmly recommended to achieve repeatable results. Moreover, flows of these materials in complex 3D geometries, which are typical in industrial practice, are insufficiently examined and in particular rheometric measurements of normal stresses are in the initial phase only (Mendes and Thompson 2019). Topics of unresolved problems in rheological investigations of Carbopol microgels, described in this review, remain to be addressed. For instance, further research is required to elucidate the importance of normal stresses and the corresponding von Mises stress in relation to the yield-stress value of the microgels. In addition, the validity of Doraiswamy et al. (1991) and Laun (1986) rules to Carbopol microgels should be carefully tested. A brief description of physical and rheological models useful in interpretation of rheological Carbopol data is presented in Table 4.

The current review has been presented separately for the chemical, physical and rheological characterization and it should be concluded that none of the cited references has dealt with all three aspects, which are important in the description of Carbopol microgels. This review represents a distinctive case of addressing the three characterization methods and it is therefore expected it can open a new path in microgel research where all three aspects are jointly considered. It follows from the discussed cases that the strongest progress in characterization of Carbopol microgels resulted hitherto from joint physical-rheological

Table 4: Models applicable to rheological characteristics of Carbopol gels.

No.	Model name	Characteristic features, equations, if cited	Main usage	Constraints	Reference
1	Herschel-Bulkley	Empirical, for yield-stress shear-dependent materials, Eq. (1-2)	Correlations of steady-state measurements	Nonuniversal model constants	Herschel and Bulkley (1926)
2	Generalized Herschel-Bulkley	Modification of H-B model in Eq. (3-4) to obtain master relationship for YSFs	Universal correlations of flow curves of YSFs	Not fully tested for different microgels	(Cloitre et al. 2003a, Bonnecaze and Cloitre 2010)
3	Additive stress	Theoretical, total stress as sum of glass, jam and solvent contributions, Eq. (3-1)	Analysis of glass-jamming crossover	Applicable to soft repulsive particles	(Ikeda et al. 2012, 2013)
4	Critical strain, polyelectrolyte	Empirical, yield stress proportional to critical strain and elastic modulus, Eqs. (3-10, 11)	Various microgel rheological data	Critical strain may be dependent on microgel type	Bhattacharjee et al. (2018)
5	Elastohydrodynamic lubrication	Balance between normal stress on particle and osmotic pressure, Eq. (3-3)	For predicting slip velocity of solid-like microgel	Shear stress much lower than yield stress	Meeker et al. (2004a)
6	Micromechanical	3D model, Eq. (3-5) for flow of soft glasses, applicable to jamming	Flow curves of yield-stress materials	Exponent of 1/2 is theoretical	(Seth et al. 2006, Seth et al. 2011)
7	Compression	Balance between elastic and compression forces, Eq. (3-7)	Estimation of Young modulus of microgels	Maximum strain of 0.36 assumed	Nordstrom et al. (2010b)
8	Elasto-viscoplastic	Rheological model with spring, 2 dashpots and solid friction element, Eq. (4-14)	Differential 3D equation for numerical modeling	Requires two additional differ. balance equations	(Saramito 2007, 2009)
9	Thixotropic- elasto-viscoplastic	Two differential constitutive equations, for shear stress and structure parameter, Eqs. (4 to (4- to -15) to 19)	Determination of the Jeffreys material functions	Limited applicability to Carbopol microgels	(Mendes 2011, Mendes and Thompson 2013)

investigations. That prevalence was also reflected in the relative number of studied papers, which were devoted to the application of two characterization methods. The number was of about 9% for the cases of physical and rheological research tools used jointly, being about two times higher than the numbers for the chemical-physical or chemical-rheological ones. Thus, the anticipated, detailed chemical characterization of the molecular structure of Carbopol microgels should enhance their molecular modeling. Similarly, based on the analysis of Lidon et al. (2017) one can predict that both residual stresses and the course of Carbopol microgel aging can be successfully explained by transformation of the chemical structure of Carbopol hydrogels. Thus, we can assume that several types of joint chemical-rheological investigations should significantly contribute to the progress in our understanding of Carbopol hydrogels. It may also be expected that a wider involvement of the chemical nanoscale characterization would render the hydrogel design more precise. Nevertheless, the described multiscale research applications of Carbopol microgels clearly allow to classify them as model yield-stress materials.

In the final conclusion, the authors would like to express encouragement to the prospective researchers of microgels to use possibly all three types of characterization of those soft-matter representatives. A joint application of all the scales of scrutiny seems to be the most promising way of future microgel research.

Acknowledgements: The authors are grateful to the anonymous reviewers for their valuable and constructive comments.

Author contributions: All the authors have accepted responsibility for the entire content of this submitted manuscript and approved submission.

Research funding: Funding of the research project No. 2017/25/B/ST8/01693 by the National Science Centre, Poland, which enabled this study, is gratefully acknowledged.

Conflict of interest statement: The authors declare no conflicts of interest regarding this article.

References

Adams, L.W. and Barigou, M. (2007). CFD analysis of caverns and pseudo-caverns developed during mixing of non-Newtonian fluids. Chem. Eng. Res. Des. 85: 598–604.

Agarwal, M., and Joshi, Y.M. (2019). Signatures of physical aging and thixotropy in aqueous dispersion of Carbopol. Phys. Fluids 31: 063107-1-063107-11.

Ahmed, E.M. (2015). Hydrogel: preparation, characterization, and applications: a review. J. Adv. Res. 6: 105–121.

Ahonguio, F., Jossic, L., and Magnin, A. (2016a). Influence of slip on the flow of a yield stress fluid around a flat plate. AIChE J. 62: 1356–1363.

Ahonguio, F., Jossic, L., Magnin, A., and Dufour, F. (2016b). Flow of an elasto-viscoplastic fluid around a flat plate: experimental and numerical data. J. Non-Newtonian Fluid Mech. 238: 131–139.

Aktas, S., Kalyon, D.M., Marin-Santibanez, B.M., and Perez-Gonzalez, J. (2014). Shear viscosity and wall slip behavior of a viscoplastic hydrogel. J. Rheol. 58: 513–535.

Alba, K., Taghavi, S.M., de Bruyn, J.R., and Frigaard, I.A. (2013). Incomplete fluid fluid displacement of yield-stress fluids. Part 2: highly inclined pipes. J. Non-Newtonian Fluid Mech. 201: 80–93.

Alberini, F., Simmons, M.J.H., Ingram, A., and Stitt, E.H. (2014). Use of an areal distribution of mixing intensity to describe blending of non-Newtonian fluids in a Kenics KM static mixer using PLIF. AIChE J 60: 332–342.

Almdal, K., Dyre, J., Hvidt, S., and Kramer, O. (1993). What is a gel. Makromol. Chem. Macromol. Symp. 76: 49–51.

Amanullah, A., Hjorth, S.A., and Nienow, A.W. (1997). Cavern sizes generated in highly shear thinning viscous fluids by SCABA 3SHP1 impellers. Food Bioprod. Process. 75: 232–238.

Arratia, P.E., Kukura, J., Lacombe, J., and Muzzio, F.J. (2006). Mixing of shear-thinning fluids with yield stress in stirred tanks. AIChE J 52: 2310–2322.

Aufderhorst-Roberts, A., Baker, D., Foster, R.J., Cayre, O., Mattsson, J., and Connell, S.D. (2018). Nanoscale mechanics of microgel particles. Nanoscale 10: 16050–16061.

Baker, W.O. (1949). Microgel, a new macromolecule - relation to sol and gel as structural elements of synthetic rubber. Ind. Eng. Chem. 41: 511–520.

Ball, R.C. and Melrose, J.R. (1995). Lubrication breakdown in hydrodynamic simulations of concentrated colloids. Adv. Colloid Interface Sci. 59: 19–30.

Balmforth, N.J., Frigaard, I.A., and Ovarlez, G. (2014). Yielding to stress: recent developments in viscoplastic fluid mechanics. Annu. Rev. Fluid Mech. 46: 121–146.

Baravian, C. and Quemada, D. (1998). Using instrumental inertia in controlled stress rheometry. Rheol. Acta 37: 223–233.

Barnes, H.A. (1995). A review of the slip (wall depletion) of polymer solutions, emulsions and particle suspensions in viscometers: its cause, character, and cure. J. Non-Newtonian Fluid Mech. 56: 221–251.

Barnes, H.A. (1999). The yield stress - a review or 'pi alpha nu tau alpha rho epsilon iota' - everything flows?. J. Non-Newtonian Fluid Mech. 81: 133–178.

Barnes, H.A. and Walters, K. (1985). The yield stress myth. Rheol. Acta 24: 323–326.

Barnes, H.A., Hutton, J.F., and Walters, K. (1993). *An introduction to rheology*. Elsevier, Amsterdam.

Barry, B.W. and Meyer, M.C. (1974). Viscoelastic and continuous shear properties of Carbopol gels. J. Pharm. Pharmacol. 26: P129–P130.

Barry, B.W. and Meyer, M.C. (1979a). Rheological properties of Carbopol gels. 1. Continuous shear and creep properties of Carbopol gels. Int. J. Pharm. 2: 1–25.

Barry, B.W. and Meyer, M.C. (1979b). Rheological properties of Carbopol gels. 2. Oscillatory properties of Carbopol gels. Int. J. Pharm. 2: 27–40.

Baudonnet, L., Pere, D., Michaud, P., Grossiord, J.L., and Rodriguez, F. (2002). Effect of dispersion stirring speed on the particle size distribution and rheological properties of carbomer dispersions and gels. J. Dispersion Sci. Technol. 23: 499–510.

Baudonnet, L., Grossiord, J.L., and Rodriguez, F. (2004). Effect of dispersion stirring speed on the particle size distribution and rheological properties of three carbomers. J. Dispersion Sci. Technol. 25: 183–192.

Benmouffok-Benbelkacem, G., Caton, F., Baravian, C., and Skali-Lami, S. (2010). Non-linear viscoelasticity and temporal behavior of typical yield stress fluids: carbopol, xanthan and ketchup. Rheol. Acta 49: 305–314.

Berney, B.M. and Deasy, P.B. (1979). Evaluation of Carbopol 934 as a suspending agent for sulfadimidine suspensions. Int. J. Pharm. 3: 73–80.

Bertola, V., Bertrand, F., Tabuteau, H., Bonn, D., and Coussot, P. (2003). Wall slip and yielding in pasty materials. J. Rheol. 47: 1211–1226.

Bhattacharjee, T., Kabb, C.P., O'Bryan, C.S., Uruena, J.M., Sumerlin, B.S., Sawyer, W.G., and Angelini, T.E. (2018). Polyelectrolyte scaling laws for microgel yielding near jamming. Soft Matter 14: 1559–1570.

Bingham, E.C. (1916). An investigation of the laws of plastic flow. Bull. Bur. Stand. 13: 309–353.

Blackwell, B.C. and Ewoldt, R.H. (2016). Non-integer asymptotic scaling of a thixotropic-viscoelastic model in large-amplitude oscillatory shear. J. Non-Newtonian Fluid Mech. 227: 80–89.

Blanksby, S.J. and Ellison, G.B. (2003). Bond dissociation energies of organic molecules. Acc. Chem. Res. 36: 255–263.

Bonn, D. and Denn, M.M. (2009). Yield stress slowly yield to analysis. Science 324: 1401–1402.

Bonn, D., Denn, M.M., Berthier, L., Divoux, T., and Manneville, S. (2017). Yield stress materials in soft condensed matter. Rev. Mod. Phys. 89, https://doi.org/10.1103/revmodphys.89.035005.

Bonnecaze, R.T. and Cloitre, M. (2010). Micromechanics of soft particle glasses. Adv. Polym. Sci. 236: 117–161.

Borrega, R., Cloitre, M., Betremieux, I., Ernst, B., and Leibler, L. (1999). Concentration dependence of the low-shear viscosity of polyelectrolyte micro-networks: from hard spheres to soft microgels. Europhys. Lett. 47: 729–735.

Borukhov, I., Andelman, D., Borrega, R., Cloitre, M., Leibler, L., and Orland, H. (2000). Polyelectrolyte titration: theory and experiment. J. Phys. Chem. B 104: 11027–11034.

Carnali, J.O. and Naser, M.S. (1992). The use of dilute solution viscometry to characterize the network properties of Carbopol microgels. Colloid Polym. Sci. 270: 183–193.

Cheddadi, I., Saramito, P., Dollet, B., Raufaste, C., and Graner, F. (2011). Understanding and predicting viscous, elastic, plastic flows. Eur. Phys. J. E 34: 1–15.

Chen, L.B. and Zukoski, C.F. (1990). Flow of ordered latex suspensions: yielding and catastrophic shear thinning. J. Chem. Soc. Faraday. Trans. 86: 2629–2639.

Christel, M., Yahya, R., Albert, M., and Antoine, B.A. (2012). Stick-slip control of the Carbopol microgels on polymethyl methacrylate transparent smooth walls. Soft Matter 8: 7365–7367.

Cloitre, M. and Bonnecaze, R.T. (2017). A review on wall slip in high solid dispersions. Rheol. Acta 56: 283–305.

Cloitre, M., Borrega, R., and Leibler, L. (2000). Rheological aging and rejuvenation in microgel pastes. Phys. Rev. Lett. 85: 4819–4822.

Cloitre, M., Borrega, R., Monti, F., and Leibler, L. (2003a). Glassy dynamics and flow properties of soft colloidal pastes. Phys. Rev. Lett. 90: 068303-1–068303-4.

Cloitre, M., Borrega, R., Monti, F., and Leibler, L. (2003b). Structure and flow of polyelectrolyte microgels: from suspensions to glasses. Compt. Rendus Phys. 4: 221–230.

Cortada-Garcia, M., Weheliye, W.H., Dore, V., Mazzei, L., and Angeli, P. (2018). Computational fluid dynamic studies of mixers for highly viscous shear thinning fluids and PIV validation. Chem. Eng. Sci. 179: 133–149.

Coussot, P. (2014). Yield stress fluid flows: a review of experimental data. J. Non-Newtonian Fluid Mech. 211: 31–49.

Coussot, P. (2017). Bingham's heritage. Rheol. Acta 56: 163–176.

Coussot, P., Nguyen, Q.D., Huynh, H.T., and Bonn, D. (2002). Viscosity bifurcation in thixotropic, yielding fluids. J. Rheol. 46: 573–589.

Coussot, P., Tabuteau, H., Chateau, X., Tocquer, L., and Ovarlez, G. (2006). Aging and solid or liquid behavior in pastes. J. Rheol. 50: 975–994.

Coussot, P., Tocquer, L., Lanos, C., and Ovarlez, G. (2009). Macroscopic vs. local rheology of yield stress fluids. J. Non-Newtonian Fluid Mech. 158: 85–90.

Coussot, P., Malkin, A.Y., and Ovarlez, G. (2017). Introduction: yield stress-or 100 years of rheology. Rheol. Acta 56: 161–162.

Cox, W.P. and Merz, E.H. (1958). Correlation of dynamic and steady flow viscosities. J. Polym. Sci. 28: 619–622.

Curran, S.J., Hayes, R.E., Afacan, A., Williams, M.C., and Tanguy, P.A. (2000). Experimental mixing study of a yield stress fluid in a laminar stirred tank. Ind. Eng. Chem. Res. 39: 195–202.

Curran, S.J., Hayes, R.E., Afacan, A., Williams, M.C., and Tanguy, P.A. (2002). Properties of carbopol solutions as models for yield-stress fluids. J. Food Sci. 67: 176–180.

Davaille, A., Gueslin, B., Massmeyer, A., and Di Giuseppe, E. (2013). Thermal instabilities in a yield stress fluid: existence and morphology. J. Non-Newtonian Fluid Mech. 193: 144–153.

Davies, G.A. and Stokes, J.R. (2008). Thin film and high shear rheology of multiphase complex fluids. J. Non-Newtonian Fluid Mech. 148: 73–87.

de Cagny, H., Fazilati, M., Habibi, M., Denn, M.M., and Bonn, D. (2019). The yield normal stress. J. Rheol. 63: 285–290.

De Gennes, P.G., Pincus, P., Velasco, R.M., and Brochard, F. (1976). Remarks on polyelectrolyte conformation. J. Physiol. Paris 37: 1461–1473.

Dekker, R.I., Dinkgreve, M., de Cagny, H., Koeze, D.J., Tighe, B.P., and Bonn, D. (2018). Scaling of flow curves: comparison between experiments and simulations. J. Non-Newtonian Fluid Mech. 261: 33–37.

Del Giudice, F., Tassieri, M., Oelschlaeger, C., and Shen, A.Q. (2017). When microrheology, bulk rheology, and microfluidics meet: broadband rheology of hydroxyethyl cellulose water solutions. Macromolecules 50: 2951–2963.

Denton, A.R., and Tang, Q.Y. (2016). Counterion-induced swelling of ionic microgels. J. Chem. Phys. 145: 164901-1–164901–10.

Di Giuseppe, E., Corbi, F., Funiciello, F., Massmeyer, A., Santimano, T.N., Rosenau, M., and Davaille, A. (2015). Characterization of Carbopol hydrogel rheology for experimental tectonics and geodynamics. Tectonophysics 642: 29–45.

Dimitriou, C.J. and McKinley, G.H. (2019). A canonical framework for modeling elasto-viscoplasticity in complex fluids. J. Non-Newtonian Fluid Mech. 265: 116–132.

Dimitriou, C.J., Ewoldt, R.H., and McKinley, G.H. (2013). Describing and prescribing the constitutive response of yield stress fluids using large amplitude oscillatory shear stress (LAOStress). J. Rheol. 57: 27–70.

Dinkgreve, M., Paredes, J., Denn, M.M., and Bonn, D. (2016). On different ways of measuring "the" yield stress. J. Non-Newtonian Fluid Mech. 238: 233–241.

Dinkgreve, M., Denn, M.M., and Bonn, D. (2017). Everything flows?": elastic effects on startup flows of yield-stress fluids. Rheol. Acta 56: 189–194.

Dinkgreve, M., Fazilati, M., Denn, M.M., and Bonn, D. (2018a). Carbopol: from a simple to a thixotropic yield stress. J. Rheol. 62: 773–780.

Dinkgreve, M., Michels, M.A.J., Mason, T.G., and Bonn, D. (2018b). Crossover between athermal jamming and the thermal glass transition of suspensions. Phys. Rev. Lett. 121: 228001-1–228001-5.

Divoux, T., Tamarii, D., Barentin, C., and Manneville, S. (2010). Transient shear banding in a simple yield stress fluid. Phys. Rev. Lett. 104: 208301-1–208301–4.

Dinkgreve, M., Paredes, J., Michels, M.A.J., and Bonn, D. (2015). Universal rescaling of flow curves for yield-stress fluids close to jamming. Phys. Rev. E 92: 012305-1-012305-17.

Divoux, T., Barentin, C., and Manneville, S. (2011a). From stress-induced fluidization processes to Herschel-Bulkley behaviour in simple yield stress fluids. Soft Matter 7: 8409–8418.

Divoux, T., Barentin, C., and Manneville, S. (2011b). Stress overshoot in a simple yield stress fluid: an extensive study combining rheology and velocimetry. Soft Matter 7: 9335–9349.

Divoux, T., Tamarii, D., Barentin, C., Teitel, S., and Manneville, S. (2012). Yielding dynamics of a Herschel-Bulkley fluid: a critical-like fluidization behaviour. Soft Matter 8: 4151–4164.

Dobrynin, A.V. (2008). Theory and simulations of charged polymers: from solution properties to polymeric nanomaterials. Curr. Opin. Colloid Interface Sci. 13: 376–388.

Dolz, M., Herraez, M., Gonzalez, F., Diez, O., Delegido, J., and Hernandez, M.J. (1998). Flow behaviour of Carbopol-940 (R) hydrogels. The influence of concentration and agitation time. Pharmazie 53: 126–130.

Doraiswamy, D., Mujumdar, A.N., Tsao, I., Beris, A.N., Danforth, S.C., and Metzner, A.B. (1991). The Cox-Merz rule extended - a rheological model for concentrated suspensions and other materials with a yield stress. J. Rheol. 35: 647–685.

Drozdov, A.D., and Christiansen, J.D. (2015). Modeling the effects of pH and ionic strength on swelling of anionic polyelectrolyte gels. Model. Simulat. Mater. Sci. Eng. 23: 055005-1-055005-38.

Drozdov, A.D., Sanporean, C.G., and Christiansen, J.D. (2016). Modeling the effect of ionic strength on swelling of pH-sensitive macro- and nanogels. Mater. Today Commun. 6: 92–101.

Dylak, A., and Jaworski, Z. (2014). A CFD study of formation of the intensive mixing zone in a highly non-Newtonian fluid. In: *International Conference on Numerical Analysis and Applied Mathematics (ICNAAM), Rhodes*, 1648. AIP Conference Proceedings, https://doi.org/10.1063/1.4912330.

Egerton, R.F. (2005). *Physical principles of electron microscopy. An introduction to TEM, SEM, and AEM*. Springer Science+Business Media, New York, USA, https://doi.org/10.1007/b136495.

Ewoldt, R.H. and McKinley, G.H. (2007). Creep ringing in rheometry or how to deal with oft-discarded data in step stress tests. Rheol. Bull. 76: 22–24.

Ewoldt, R.H., Hosoi, A.E., and McKinley, G.H. (2008). An ontology for large amplitude oscillatory shear flow. In: *15th International Congress on Rheology/80th Annual Meeting of the Society-of-Rheology, Monterey*, 1027. AIP Conference Proceedings, pp. 1135–1137.

Ewoldt, R.H., Winter, P., Maxey, J., and McKinley, G.H. (2010). Large amplitude oscillatory shear of pseudoplastic and elastoviscoplastic materials. Rheol. Acta 49: 191–212.

Fall, A., Paredes, J., and Bonn, D. (2010). Yielding and shear banding in soft glassy materials. Phys. Rev. Lett. 105, https://doi.org/10.1103/physrevlett.105.225502.

Fischer, W.H., Bauer, W.H., and Wiberley, S.E. (1961). Yield stresses and flow properties of carboxypolymethylene-water systems. Trans. Soc. Rheol. 5: 221–235.

Flory, P.J. and Rehner, J. (1943). Statistical mechanics of cross-linked polymer networks II Swelling. J. Chem. Phys. 11: 521–526.

Fraggedakis, D., Dimakopoulos, Y., and Tsamopoulos, J. (2016). Yielding the yield stress analysis: a thorough comparison of recently proposed elasto-visco-plastic (EVP) fluid models. J. Non-Newtonian Fluid Mech. 238: 170–188.

Frigaard, I. (2019). Simple yield stress fluids. Curr. Opin. Colloid Interface Sci. 43: 80–93.

Genani, E. and Powell, R.L. (1985). Transient flow viscometry. J. Rheol. 29: 931–941.

Geraud, B., Bocquet, L., and Barentin, C. (2013). Confined flows of a polymer microgel. Eur. Phys. J. E. 36, https://doi.org/10.1140/epje/i2013-13030-3.

Géraud, B., Jorgensen, L., Ybert, C., Delanoe-Ayari, H., and Barentin, C. (2017). Structural and cooperative length scales in polymer gels. Eur. Phys. J. E 40: 1–10.

Gomez-Carracedo, A., Alvarez-Lorenzo, C., Gomez-Amoza, J.L., and Concheiro, A. (2004). Glass transitions and viscoelastic properties of Carbopol (R) and Noveon (R) compacts. Int. J. Pharm. 274: 233–243.

Gomez, C., Derakhshandeh, B., Hatzikiriakos, S.G., and Bennington, C.P.J. (2010). Carbopol as a model fluid for studying mixing of pulp fibre suspensions. Chem. Eng. Sci. 65: 1288–1295.

Gutowski, I.A., Lee, D., de Bruyn, J.R., and Frisken, B.J. (2012). Scaling and mesostructure of Carbopol dispersions. Rheol. Acta 51: 441–450.

Habibi, M., Dinkgreve, M., Paredes, J., Denn, M.M., and Bonn, D. (2016). Normal stress measurement in foams and emulsions in the presence of slip. J. Non-Newtonian Fluid Mech. 238: 33–43.

Harrington, J.C. (2012). The effects of neutralization on the dynamic rheology of polyelectrolyte microgel mucilages. J. Appl. Polym. Sci. 126: 770–777.

Hassan, M.A., Pathak, M., and Khan, M.K. (2015). Thermorheological characterization of elastoviscoplastic Carbopol Ultrez 20 gel. J. Dispersion Sci. Technol. 137, https://doi.org/10.1115/1.4030004.

Hedrick, M.M., Chung, J.K., and Denton, A.R. (2015). Structure and osmotic pressure of ionic microgel dispersions. J. Chem. Phys. 142: 034904-1-034904-12.

Hernandez, M.T., Pellicer, J., Delegido, J., and Dolz, M. (1998). Rheological characterization of easy-to-disperse (ETD) Carbopol hydrogels. J. Dispersion Sci. Technol. 19: 31–42.

Herschel, W.H. and Bulkley, R. (1926). Consistency measurements of rubber-benzol solutions. Kolloid Z. 39: 291–300.

Herth, G., Schornick, G., and Buchholz, F.L. (2016). *Polyacrylamides and poly(acrylic acid)s, 2*, Organics polymers ed. Wiley-VCH, Hamburg.

Hirata, Y., Nienow, A.W., and Moore, I.P.T. (1994). Estimation of cavern sizes in a shear-thinning plastic fluid agitated by a Rushton turbine based on LDA measurements. J. Chem. Eng. Jpn. 27: 235–237.

Hoare, T. and Pelton, R. (2004). Functional group distributions in carboxylic acid containing poly(N-isopropylacrylamide) microgels. Langmuir 20: 2123–2133.

Hoare, T. and Pelton, R. (2007). Functionalized microgel swelling: comparing theory and experiment. J. Phys. Chem. B 111: 11895–11906.

Hoare, T. and Pelton, R. (2008). Characterizing charge and crosslinker distributions in polyelectrolyte microgels. Curr. Opin. Colloid Interface Sci. 13: 413–428.

Holenberg, Y., Lavrenteva, O.M., Shavit, U., and Nir, A. (2012). Particle tracking velocimetry and particle image velocimetry study of the slow motion of rough and smooth solid spheres in a yield-stress fluid. Phys. Rev. E 86: 066301-1-066301-6.

Hsu, C.C. (1997). Polycarboxylic acid with higher thickening capacity and better clarity, Patent no. 4923940. US Patent.

Hyun, K., Wilhelm, M., Klein, C.O., Cho, K.S., Nam, J.G., Ahn, K.H., Lee, S.J., Ewoldt, R.H., and McKinley, G.H. (2011). A review of nonlinear oscillatory shear tests: analysis and application of large amplitude oscillatory shear (LAOS). Prog. Polym. Sci. 36: 1697–1753.

Ikeda, A., Berthier, L., and Sollich, P. (2012). Unified study of glass and jamming rheology in soft particle systems. Phys. Rev. Lett. 109: 018301-1-018301-5.

Ikeda, A., Berthier, L., and Sollich, P. (2013). Disentangling glass and jamming physics in the rheology of soft materials. Soft Matter 9: 7669–7683.

Islam, M.T., Rodriguez-Hornedo, N., Ciotti, S., and Ackermann, C. (2004). Rheological characterization of topical carbomer gels neutralized to different pH. Pharm. Res. 21: 1192–1199.

IUPAC (1997). *IUPAC. Compendium of chemical terminology*, 2nd (the Gold Book) ed. Blackwell Scientific Publications, Oxford.

Jimenez, M.M., Fresno, M.J., and Ramirez, A. (2007). Rheological study of binary gels with Carbopol (R) Ultre (TM) 10 and hyaluronic acid. Chem. Pharmaceut. Bull. 55: 1157–1163.

Jofore, B.D., Erni, P., Vleminckx, G., Moldenaers, P., and Clasen, C. (2015). Rheology of microgels in single particle confinement. Rheol. Acta 54: 581–600.

Joshi, Y.M. and Petekidis, G. (2018). Yield stress fluids and ageing. Rheol. Acta 57: 521–549.

Kaberova, Z., Karpushkin, E., Nevoralova, M., Vetrik, M., Slouf, M., and Duskova-Smrckova, M. (2020). Microscopic structure of swollen hydrogels by scanning electron and light microscopies: artifacts and reality. Polymers 12: 578-1–578–18.

Kalyon, D.M. (2005). Apparent slip and viscoplasticity of concentrated suspensions. J. Rheol. 49: 621–640.

Kawaguchi, S., Yekta, A., and Winnik, M.A. (1995). Surface characterization and dissociation properties of carboxylic acid core-shell latex particle by potentiometric and conductometric titration. J. Colloid Interface Sci. 176: 362–369.

Kelessidis, V.C. and Hatzistamou, V. (2011). Preparation methodology and rheological properties of yield pseudoplastic transparent fluids. J. Dispersion Sci. Technol. 32: 380–388.

Ketz, R.J., Prudhomme, R.K., and Graessley, W.W. (1988). Rheology of concentrated microgel solutions. Rheol. Acta 27: 531–539.

Khokhlov, A.R. and Khachaturian, K.A. (1982). On the theory of weakly charged polyelectrolytes. Polymer 23: 1742–1750.

Khokhlov, A.R. and Kramarenko, E.Y. (1996). Weakly charged polyelectrolytes: collapse induced by extra ionization. Macromolecules 29: 681–685.

Kiljański, T. (1989). A method for correction of the wall-slip effect in a Couette rheometer. Rheol. Acta 28: 61–64.

Kim, J.Y., Song, J.Y., Lee, E.J., and Park, S.K. (2003). Rheological properties and microstructures of Carbopol gel network system. Colloid Polym. Sci. 281: 614–623.

Koch, M. and Włodarczyk-Biegun, M.K. (2020). Faithful scanning electron microscopic (SEM) visualization of 3D printed alginate-based scaffolds. Bioprinting 20: 1–20.

Konop, A.J. and Colby, R.H. (1999). Polyelectrolyte charge effects on solution viscosity of poly(acrylic acid). Macromolecules 32: 2803–2805.

Kramarenko, E.Y., Khokhlov, A.R., and Yoshikawa, K. (1997). Collapse of polyelectrolyte macromolecules revisited. Macromolecules 30: 3383–3388.

Kramarenko, E.Y., Philippova, O.E., and Khokhlov, A.R. (2006). Polyelectrolyte networks as highly sensitive polymers. Polym. Sci. Ser. C 48: 1–20.

Labanda, J., Marco, P., and Llorens, J. (2004). Rheological model to predict the thixotropic behaviour of colloidal dispersions. Colloids Surf, A 249: 123–126.

Laun, H.M. (1986). Prediction of elastic strains of polymer melts in shear and elongation. J. Rheol. 30: 459–501.

Lee, D., Gutowski, I.A., Bailey, A.E., Rubatat, L., de Bruyn, J.R., and Frisken, B.J. (2011). Investigating the microstructure of a yield-stress fluid by light scattering. Phys. Rev. E 83, https://doi.org/10.1103/physreve.83.031401.

Lefrancois, P., Ibarboure, E., Payre, B., Gontier, E., Le Meins, J.F., and Schatz, C. (2015). Insights into Carbopol gel formulations: microscopy analysis of the microstructure and the influence of polyol additives. J. Appl. Polym. Sci. 132, https://doi.org/10.1002/app.42761.

Leite, R.T., Mendes, P.R.D., and Thompson, R.L. (2019). A simple method to analyze materials under quasilinear large amplitude oscillatory shear flow (QL-LAOS). J. Rheol. 63: 305–317.

Leong, Y.K., Campbell, G.R., Yeow, Y.L., and Withers, J.W. (2008). Processing parallel-disk viscometry data in the presence of wall slip. Korea Aust. Rheol. J. 20: 51–58.

Li, B., Xu, L., Wu, Q., Chen, T., Sun, P., Jin, Q., Ding, D., Wang, X., Xue, G., and Shi, A.C. (2007). Various types of hydrogen bonds, their temperature dependence and water-polymer interaction in hydrated poly(acrylic acid) as revealed by H-1 solid-state NMR spectroscopy. Macromolecules 40: 5776–5786.

Li, J.Y., Suo, Z.G., and Vlassak, J.J. (2014). A model of ideal elastomeric gels for polyelectrolyte gels. Soft Matter 10: 2582–2590.

Li, S.P., Zhao, G., and Chen, H.Y. (2005). The relationship between steady shear viscosity and complex viscosity. J. Dispersion Sci. Technol. 26: 415–419.

Lidon, P., Villa, L., and Manneville, S. (2017). Power-law creep and residual stresses in a carbopol gel. Rheol. Acta 56: 307–323.

Lifshitz, I.M., Grosberg, A.Y., and Khokhlov, A.R. (1978). Some problems of statistical physics of polymer chains with volume interaction. Rev. Mod. Phys. 50: 683–713.

Liu, K., Cruzan, J.D., and Saykally, R.J. (1996). Water clusters. Science 271: 929–933.

Liu, W.W., Peng, J., Zhu, K.Q., and Zhang, J.J. (2016). A microstructural criterion for yielding: linking thixotropy and the yield stress. Rheol. Acta 55: 957–968.

Liu, Y., Lorusso, D., Holdsworth, D.W., Poepping, T.L., and de Bruyn, J.R. (2018). Effect of confinement on the rheology of a yield-stress fluid. J. Non-Newtonian Fluid Mech. 261: 25–32.

Lochhead, R.Y. (2017). *The use of polymers in cosmetic products*. Elsevier, Amsterdam.

Lodge, A.S. (1975). Stress relaxation after a sudden shear strain. Rheol. Acta 14: 664–665.

Lodge, A.S. and Meissner, J. (1972). On the use of instantaneous strains, superposed on shear and elongational flows of polymeric liquids, to test the Gaussian network hypothesis and to estimate the segment concentration and its variation during flow. Rheol. Acta 11: 351–352.

Louvet, N., Bonn, D., and Kellay, H. (2014). Nonuniversality in the pinch-off of yield stress fluids: role of nonlocal rheology. Phys. Rev. Lett. 113, https://doi.org/10.1103/physrevlett.113.218302.

Lubrizol (2007). TDS-222 molecular weight of Carbopol® and Pemulen® polymers, Available at: https://www.lubrizol.com/-/media/Lubrizol/Life-Sciences/Documents/TDS/Molecular-Weight-of-Carbopol-and-Pemulen.pdf (Accessed 12 July 2018).

Lubrizol (2008). Carbopol polymers: overview, Available at: https://pl.scribd.com/document/158844643/Carbopol-Polymer-Powder (Accessed 12 July 2018).

Lubrizol (2009). Technical data sheet (TDS-237). Neutralizing Carbopol®* and Pemulen™* polymers in aqueous and hydroalcoholic systems, Available at: https://www.lubrizol.com/-/media/Lubrizol/Life-Sciences/Documents/TDS/Neutralizing-Carbopol-and-Pemeulen-in-Aqueous-and-Hydroalcoholic-Systems.pdf (Accessed 10 January 2019).

Lubrizol (2018a). Carbopol® polymer products - Lubrizol, Available at: https://www.lubrizol.com/Life-Sciences/Products/Carbopol-Polymer-Products (Accessed 12 July 2018).

Lubrizol (2018b). Pharmaceutical polymers typical properties and specifications, Available at: https://www.lubrizol.com/-/media/Lubrizol/Life-Sciences/Documents/Literature/Brochure/Pharmaceutical-Polymers-Typical-Properties-and-Specifications.pdf (Accessed 21 July 2018).

Macosko, C.W. (1994). *Rheology principles, measuremets, and applications*. Wiley-VCH, New York.

Macsporran, W.C. and Spiers, R.P. (1982a). The dynamic performance of the Weissenberg rheogoniometer I. Small amplitude oscillatory shearing. Rheol. Acta 21: 184–192.

Macsporran, W.C. and Spiers, R.P. (1982b). The dynamic performance of the Weissenberg rheogoniometer II. Large amplitude oscillatory shearing - fundamental response. Rheol. Acta 21: 193–200.

Magnin, A., and Piau, J.M. (1990). Cone-and-plate rheometry of yield stress fluids. Study of an aqueous gel. J. Non-Newtonian Fluid Mech. 36: 85–108.

Malkin, A., Kulichikhin, V., and Ilyin, S. (2017). A modern look on yield stress fluids. Rheol. Acta 56: 177–188.

Malkin, A.Y. and Isayev, A.I. (2006). *Rheology concepts, methods, & application*. ChemTec Publishing, Toronto.

Malkin, A.Y. and Patlazhan, S.A. (2018). Wall slip for complex liquids - phenomenon and its causes. Adv. Colloid Interface Sci. 257: 42–57.

Manogaran, D. (2019). Making and breaking of small water clusters: a combined quantum chemical and molecular dynamics approach. J. Comput. Chem. 40: 1556–1569.

Manzo, R.H., Jimenez-Kairuz, A.F., Olivera, M.E., Alovero, F., and Ramirez-Rigo, M.V. (2014). Thermodynamic and rheological properties of polyelectrolyte systems. Polyelectrolytes: Therm. Rheol.: 215–244, https://doi.org/10.1007/978-3-319-01680-1_6.

Marcus, R.A. (1955). Calculation of thermodynamic properties of polyelectrolytes. J. Chem. Phys. 23: 1057–1068.

Mattsson, J. (2016). *The glass transition*, 1st ed. Wiley, Hoboken, NJ.

Meeker, S.P., Bonnecaze, R.T., and Cloitre, M. (2004a). Slip and flow in pastes of soft particles: direct observation and rheology. J. Rheol. 48: 1295–1320.

Meeker, S.P., Bonnecaze, R.T., and Cloitre, M. (2004b). Slip and flow in soft particle pastes. Phys. Rev. Lett. 92: 198302.

Mendes, P.R.D. (2009). Modeling the thixotropic behavior of structured fluids. J. Non-Newtonian Fluid Mech. 164: 66–75.

Mendes, P.R.D. (2011). Thixotropic elasto-viscoplastic model for structured fluids. Soft Matter 7: 2471–2483.

Mendes, P.R.D. and Thompson, R.L. (2013). A unified approach to model elasto-viscoplastic thixotropic yield-stress materials and apparent yield-stress fluids. Rheol. Acta 52: 673–694.

Mendes, P.R.D. and Thompson, R.L. (2019). Time-dependent yield stress materials. Curr. Opin. Colloid Interface Sci. 43: 15–25.

Mendes, P.R.D., Alicke, A.A., and Thompson, R.L. (2014a). Parallel-plate geometry correction for transient rheometric experiments. Appl. Rheol. 24: 52721-1–52721-3.

Mendes, P.R.D., Thompson, R.L., Alicke, A.A., and Leite, R.T. (2014b). The quasilinear large-amplitude viscoelastic regime and its significance in the rheological characterization of soft matter. J. Rheol. 58: 537–561.

Metivier, C., Li, C., and Magnin, A. (2017). Origin of the onset of Rayleigh-Benard convection in a concentrated suspension of microgels with a yield stress behavior. Phys. Fluids 29: 104102-1–104102–10.

Mewis, J. and Wagner, N.J. (2009). Thixotropy. Adv. Colloid Interface Sci. 147-48: 214–227.

Mewis, J. and Wagner, N.J. (2012). *Colloidal suspension rheology*. Cambridge University Press, Cambridge, UK.

Michaeli, I. and Katchalsky, A. (1957). Potentiometric titration of polyelectrolyte gels. J. Polym. Sci. 23: 683–696.

Mohan, L., Pellet, C., Cloitre, M., and Bonnecaze, R. (2013). Local mobility and microstructure in periodically sheared soft particle glasses and their connection to macroscopic rheology. J. Rheol. 57: 1023–1046.

Moller, P., Fall, A., and Bonn, D. (2009a). Origin of apparent viscosity in yield stress fluids below yielding. Europhys. Lett. 87: 38004-1–38004-6.

Moller, P., Fall, A., Chikkadi, V., Derks, D., and Bonn, D. (2009b). An attempt to categorize yield stress fluid behaviour. Philos. T. R. Soc. A 367: 5139–5155.

Moller, P.C.F., Mewis, J., and Bonn, D. (2006). Yield stress and thixotropy: on the difficulty of measuring yield stresses in practice. Soft Matter 2: 274–283.

Montero, L.A., Molina, J., and Fabian, J. (2000). Multiple minima hypersurfaces of water clusters for calculations of association energy. Int. J. Quant. Chem. 79: 8–16.

Moore, I.P.T., Cossor, G., and Baker, M.R. (1995). Velocity distributions in a stirred tank containing a yield stress fluid. Chem. Eng. Sci. 50: 2467–2481.

Muramatsu, M., Kanada, K., Nishida, A., Ouchi, K., Saito, N., Yoshida, M., Shimoaka, A., Ozeki, T., Yuasa, H., and Kanaya, Y. (2000). Application of Carbopol (R) to controlled release preparations I. Carbopol (R) as a novel coating material. Int. J. Pharm. 199: 77–83.

Muthukumar, M. (2017). 50th Anniversary perspective: a perspective on polyelectrolyte solutions. Macromolecules 50: 9528–9560.

Nelson, A.Z., Bras, R.E., Liu, J.P., and Ewoldt, R.H. (2018). Extending yield-stress fluid paradigms. J. Rheol. 62: 357–369.

Nigro, V., Angelini, R., Bertoldo, M., and Ruzicka, B. (2017). Swelling behavior in multi-responsive microgels. Colloids Surf, A 532: 389–396.

Nisato, G., Schosseler, F., and Candau, S.J. (1996). Swelling equilibrium properties of partially charged gels: the effect of salt on the shear modulus. Polym. Gels Netw. 4: 481–498.

Nordstrom, K.N., Verneuil, E., Arratia, P.E., Basu, A., Zhang, Z., Yodh, A.G., Gollub, J.P., and Durian, D.J. (2010a). Microfluidic rheology of soft colloids above and below jamming. Phys. Rev. Lett. 105: 175701-1–175701-4.

Nordstrom, K.N., Verneuil, E., Ellenbroek, W.G., Lubensky, T.C., Gollub, J.P., and Durian, D.J. (2010b). Centrifugal compression of soft particle packings: theory and experiment. Phys. Rev. E 82, https://doi.org/10.1103/physreve.82.041403.

Oppong, F.K. and de Bruyn, J.R. (2007). Diffusion of microscopic tracer particles in a yield-stress fluid. J. Non-Newtonian Fluid Mech. 142: 104–111.

Oppong, F.K., and de Bruyn, J.R. (2011). Microrheology and jamming in a yield-stress fluid. Rheol. Acta 50: 317–326.

Ortega-Avila, J.F., Perez-Gonzalez, J., Marin-Santibanez, B.M., Rodriguez-Gonzalez, F., Aktas, S., Malik, M., and Kalyon, D.M. (2016). Axial annular flow of a viscoplastic microgel with wall slip. J. Rheol. 60: 503–515.

Ovarlez, G., Rodts, S., Chateau, X., and Coussot, P. (2009). Phenomenology and physical origin of shear localization and shear banding in complex fluids. Rheol. Acta 48: 831–844.

Ovarlez, G., Cohen-Addad, S., Krishan, K., Goyon, J., and Coussot, P. (2013). On the existence of a simple yield stress fluid behavior. J. Non-Newtonian Fluid Mech. 193: 68–79.

Panzade, P. and Puranik, P.K. (2010). Carbopol polymers: a verstile polymer for pharmaceutical applications. Res. J. Pharm. Technol. 3: 672–675.

Paredes, J., Michels, M.A.J., and Bonn, D. (2013). Rheology across the zero-temperature jamming transition. Phys. Rev. Lett. 111, https://doi.org/10.1103/physrevlett.111.015701.

Patel, M., Patel, B., Patel, R., Patel, J., Bharadia, P., and Patel, M. (2006). Carbopol: a versatile polymer. Drug Deliv. Technol. 6: 32–43.

Peixinho, J., Desaubry, C., and Lebouche, M. (2008). Heat transfer of a non-Newtonian fluid (Carbopol aqueous solution) in transitional pipe flow. Int. J. Heat Mass Tran. 51: 198–209.

Pemeja, J., Geraud, B., Barentin, C., and Le Merrer, M. (2019). Wall slip regimes in jammed suspensions of soft microgels. Phys. Rev. Fluids 4, https://doi.org/10.1103/physrevfluids.4.033301.

Perge, C., Taberlet, N., Gibaud, T., and Manneville, S. (2014). Time dependence in large amplitude oscillatory shear: a rheo-ultrasonic study of fatigue dynamics in a colloidal gel. J. Rheol. 58: 1331–1357.

Piau, J.M. (2007). Carbopol gels: elastoviscoplastic and slippery glasses made of individual swollen sponges Meso- and macroscopic properties, constitutive equations and scaling laws. J. Non-Newtonian Fluid Mech. 144: 1–29.

Poumaere, A., Moyers-Gonzalez, M., Castelain, C., and Burghelea, T. (2014). Unsteady laminar flows of a Carbopol (R) gel in the presence of wall slip. J. Non-Newtonian Fluid Mech. 205: 28–40.

Prasad, V., Trappe, V., Dinsmore, A.D., Segre, P.N., Cipelletti, L., and Weitz, D.A. (2003). Universal features of the fluid to solid transition for attractive colloidal particles. Faraday Discuss 123: 1–12.

Pusey, P.N. and Vanmegen, W. (1986). Phase behavior of concentrated suspensions of nearly hard colloidal spheres. Nature 320: 340–342.

Pusey, P.N. and Vanmegen, W. (1987). Observation of a glass transition in suspensions of spherical colloidal particles. Phys. Rev. Lett. 59: 2083–2086.

Putz, A.M.V. and Burghelea, T.I. (2009). The solid-fluid transition in a yield stress shear thinning physical gel. Rheol. Acta 48: 673–689.

Rabideau, B.D., Lanos, C., and Coussot, P. (2009). An investigation of squeeze flow as a viable technique for determining the yield stress. Rheol. Acta 48: 517–526.

Roberts, G.P. and Barnes, H.A. (2001). New measurements of the flow-curves for Carbopol dispersions without slip artefacts. Rheol. Acta 40: 499–503.

Rodriguez, B.E., Wolfe, M.S., and Fryd, M. (1994). Nonuniform swelling of alkali swellable microgels. Macromolecules 27: 6642–6647.

Romeo, G., Imperiali, L., Kim, J.W., Fernandez-Nieves, A., and Weitz, D.A. (2012). Origin of de-swelling and dynamics of dense ionic microgel suspensions. J. Chem. Phys. 136, https://doi.org/10.1063/1.3697762.

Rubinstein, M. and Colby, R.H. (1994). Elastic modulus and equilibrium swelling of near-critical gels. Macromolecules 27: 3184–3190.

Rubinstein, M., Colby, R.H., Dobrynin, A.V., and Joanny, J.F. (1996). Elastic modulus and equilibrium swelling of polyelectrolyte gels. Macromolecules 29: 398–406.

Rumyantsev, A.M., Pan, A., Roy, S.G., De, P., and Kramarenko, E.Y. (2016). Polyelectrolyte gel swelling and conductivity vs counterion type, cross-linking density, and solvent polarity. Macromolecules 49: 6630–6643.

Russell, A.W., Kahouadji, L., Mirpuri, K., Quarmby, A., Piccione, P.M., Matar, O.K., Luckham, P.F., and Markides, C.N. (2019). Mixing viscoplastic fluids in stirred vessels over multiple scales: a combined experimental and CFD approach. Chem. Eng. Sci. 208, https://doi.org/10.1016/j.ces.2019.07.047.

Sakurai, M., Imai, T., Yamashita, F., Nakamura, K., Komatsu, T., and Nakagawa, T. (1993). Temperature dependence of viscosities and potentiometric titration behavior of aqueous poly(acrylic acid) and poly(methacrylic acid) solutions. Polym. J. 25: 1247–1255, dslkw.

Saramito, P. (2007). A new constitutive equation for elastoviscoplastic fluid flows. J. Non-Newtonian Fluid Mech. 145: 1–14.

Saramito, P. (2009). A new elastoviscoplastic model based on the Herschel-Bulkley viscoplastic model. J. Non-Newtonian Fluid Mech. 158: 154–161.

Saramito, P. and Wachs, A. (2017). Progress in numerical simulation of yield stress fluid flows. Rheol. Acta 56: 211–230.

Saunders, B.R. and Vincent, B. (1999). Microgel particles as model colloids: theory, properties and applications. Adv. Colloid Interface Sci. 80: 1–25.

Sausset, F., Biroli, G., and Kurchan, J. (2010). Do solids flow?. J. Stat. Phys. 140: 718–727.

Sciortino, F. (2002). Disordered materials - one liquid, two glasses. Nat. Mater. 1: 145–146.

Seth, J.R., Cloitre, M., and Bonnecaze, R.T. (2006). Elastic properties of soft particle pastes. J. Rheol. 50: 353–376.

Seth, J.R., Cloitre, M., and Bonnecaze, R.T. (2008). Influence of short-range forces on wall-slip in microgel pastes. J. Rheol. 52: 1241–1268.

Seth, J.R., Locatelli-Champagne, C., Monti, F., Bonnecaze, R.T., and Cloitre, M. (2012). How do soft particle glasses yield and flow near solid surfaces?. Soft Matter 8: 140–148.

Seth, J.R., Mohan, L., Locatelli-Champagne, C., Cloitre, M., and Bonnecaze, R.T. (2011). A micromechanical model to predict the flow of soft particle glasses. Nat. Mater. 10: 838–843.

Shafiei, M., Bryant, S., Balhoff, M., Huh, C., and Bonnecaze, R.T. (2017). Hydrogel formulation for sealing cracked wellbores for CO2 storage. Appl. Rheol. 27.

Shafiei, M., Balhoff, M., and Hayman, N.W. (2018). Chemical and microstructural controls on viscoplasticity in Carbopol hydrogel. Polymer 139: 44–51.

Sharma, V. and McKinley, G.H. (2012). An intriguing empirical rule for computing the first normal stress difference from steady shear viscosity data for concentrated polymer solutions and melts. Rheol. Acta 51: 487–495.

Sollich, P. (1998). Rheological constitutive equation for a model of soft glassy materials. Phys. Rev. E. 58: 738–759.

Sollich, P. (2006). Soft glassy rheology. In: Weiss, R.G. and Terech, P. (Eds.), *Molecular gels: materials with self-assembled fibriliar networks*. Springer, Dordrecht, The Netherlands, pp. 161–192.

Sollich, P. and Cates, M.E. (2012). Thermodynamic interpretation of soft glassy rheology models. Phys. Rev. E. 85, https://doi.org/10.1103/physreve.85.031127.

Sperling, L.H. (2006). *Introduction to physical polymer science*, 4th ed. John Wiley and Sons Inc., Hoboken, New Jersey.

Story, A. and Jaworski, Z. (2017). A new model of cavern diameter based on a validated CFD study on stirring of a highly shear-thinning fluid. Chem. Pap. 71: 1255–1269.

Syrakos, A., Dimakopoulos, Y., and Tsamopoulos, J. (2020). A finite volume method for the simulation of elastoviscoplastic flows and its application to the lid-driven cavity case. J. Non-Newtonian Fluid Mech. 275, https://doi.org/10.1016/j.jnnfm.2019.104216.

Szabo, B., Suvegh, K., and Zelko, R. (2011). Effect of storage on microstructural changes of Carbopol polymers tracked by the combination of positron annihilation lifetime spectroscopy and FT-IR spectroscopy. Int. J. Pharm. 416: 160–163.

Taghavi, S.M., Alba, K., Moyers-Gonzalez, M., and Frigaard, I.A. (2012). Incomplete fluid-fluid displacement of yield stress fluids in near-horizontal pipes: experiments and theory. J. Non-Newtonian Fluid Mech. 167: 59–74.

Tan, B.H. and Tam, K.C. (2008). Review on the dynamics and microstructure of pH-responsive nano-colloidal systems. Adv. Colloid Interface Sci. 136: 25–44.

Tan, B.H., Tam, K.C., Dupin, D., and Armes, S.P. (2010). Rheological behavior of acid-swellable cationic copolymer latexes. Langmuir 26: 2736–2744.

Tan, B.H., Tam, K.C., Lam, Y.C., and Tan, C.B. (2004). A semi-empirical approach for modeling charged soft microgel particles. J. Rheol. 48: 915–926.

Taylor, N.W. and Bagley, E.B. (1974). Dispersions or solutions - mechanism for certain thickening agents. J. Appl. Polym. Sci. 18: 2747–2761.

Taylor, N.W. and Bagley, E.B. (1975). Rheology of dispersions of swollen gel particles. J. Polym. Sci, Polym. Phys. Ed. 13: 1133–1144.

Taylor, N.W. and Gordon, S.H. (1982). Shear modulus in closely packed gel suspensions. J. Appl. Polym. Sci. 27: 4377–4386.

Tessarolli, F.G.C., Queiros, Y.G.D., and Mansur, C.R.E. (2014). Evaluation of pH-sensitive hydrogels to control the permeability anisotropy of oil reservoirs. J. Appl. Polym. Sci. 131.

Testa, B. and Etter, J.C. (1972). Dissociation constants and activity coefficients for Carbopol during their potentiometric titration. Pharm. Acta Helv. 47: 438–448.

Testa, B., and Etter, J.C. (1973). Report concerning rheology used to study interactions between Carbopol macromolecules as well as semiquantitative determination of ionic force of their dispersions. Pharm. Acta Helv. 48: 378–388.

Testa, B. and Etter, J.C. (1974). Potentiometric study of Carbopol 940 hydrogels neutralized with some basic active principles. Farm. Ed. Sci. 24: 398–404.

Testa, B. and Etter, J.C. (1976). Macromolecular interactions in polyelectrolyte solutions as studied by conductimetry and surface tension techniques. Pharm. Acta Helv. 51: 253–257.

Thomas, J.B., Creecy, C.M., McGinity, J.W., and Peppas, N.A. (2006). Synthesis and properties of lightly crosslinked poly((meth) acrylic acid) microparticles prepared by free radical precipitation polymerization. Polym. Bull. 57: 11–20.

Thompson, R.L., Sica, L.U.R., and Mendes, P.R.D. (2018). The yield stress tensor. J. Non-Newtonian Fluid Mech. 261: 211–219.

Toplak, T., Tabuteau, H., de Bruyn, J.R., and Coussot, P. (2007). Gravity draining of a yield-stress fluid through an orifice. Chem. Eng. Sci. 62: 6908–6913.

Uhlherr, P.H.T., Guo, J., Tiu, C., Zhang, X.M., Zhou, J.Z.Q., and Fang, T.N. (2005). The shear-induced solid-liquid transition in yield stress materials with chemically different structures. J. Non-Newtonian Fluid Mech. 125: 101–119.

Varges, P.R., Costa, C.M., Fonseca, B.S., Naccache, M.F., and Mendes, P.R.D. (2019). Rheological characterization of Carbopol(R) dispersions in water and in water/glycerol solutions. Fluids 4.

Voigtmann, T. (2014). Nonlinear glassy rheology. Curr. Opin. Colloid Interface Sci. 19: 549–560.

Waigh, T.A. (2016). Advances in the microrheology of complex fluids. Rep. Prog. Phys. 79, https://doi.org/10.1088/0034-4885/79/7/074601.

Waisbord, N., Stoop, N., Walkama, D.M., Dunkel, J., and Guasto, J.S. (2019). Anomalous percolation flow transition of yield stress fluids in porous media. Phys. Rev. Fluids 4, https://doi.org/10.1103/physrevfluids.4.063303.

Weber, E., Moyers-Gonzalez, M., and Burghelea, T.I. (2012). Thermorheological properties of a Carbopol gel under shear. J. Non-Newtonian Fluid Mech. 183: 14–24.

Yataghene, M. and Legrand, J. (2013). A 3D-CFD model thermal analysis within a scraped surface heat exchanger. Comput. Fluids 71: 380–399.
Yoshimura, A.S. and Prud'homme, R.K. (1988). Wall slip effects on dynamic oscillatory measurements. J. Rheol. 32: 575–584.
Yoshimura, A.S., Prud'homme, R.K., Princen, H.M., and Kiss, A.D. (1987). A comparison of techniques for measuring yield stresses. J. Rheol. 31: 699–710.
Younes, E., Bertola, V., Castelain, C., and Burghelea, T. (2020a). Slippery flows of a Carbopol gel in a microchannel. Phys. Rev. Fluids 5, https://doi.org/10.1103/physrevfluids.5.083303.
Younes, E., Himl, M., Stary, Z., Bertola, V., and Burghelea, T. (2020b). On the elusive nature of Carbopol gels: "model", weakly thixotropic, or time-dependent viscoplastic materials?. J. Non-Newtonian Fluid Mech. 281, https://doi.org/10.1016/j.jnnfm.2020.104315.

Bionotes

Zdzisław Jaworski
Faculty of Chemical Technology and Engineering, West Pomeranian University of Technology, Aleja Piastow 42, 71-065, Szczecin, Poland
Zdzislaw.Jaworski@zut.edu.pl

Zdzisław Jaworski is Professor em. of West Pomeranian University of Technology, Szczecin, Poland. His research interest include chemical engineering, multiscale modeling of product engineering, computational fluid dynamics in process design, mixing and reaction technology, multiphase fluid flow, rheology, and laser velocity measurements.

Tadeusz Spychaj
Faculty of Chemical Technology and Engineering, West Pomeranian University of Technology, Aleja Piastow 42, 71-065, Szczecin, Poland
Tadeusz.Spychaj@zut.edu.pl

Prof. Tadeusz Spychaj is a former full professor of Chemical Technology and Material Engineering at Faculty of Chemical Technology and Engineering, West Pomeranian University of Technology, Szczecin, Poland. His specialization is polymer technology and engineering [reactive polymers and resins, hydrophilic polymers and gels, polymer modification, feedstock/chemical recycling of waste polymers, polymer (nano)composites/(nano)coatings, starch – based polymers, ionic liquids and deep eutectic solvents as polymer modifiers]. In 1999 he was awarded the degree of professor by the President of the Republic of Poland.

Anna Story
Faculty of Chemical Technology and Engineering, West Pomeranian University of Technology, Aleja Piastow 42, 71-065, Szczecin, Poland
Anna.Story@zut.edu.pl

Anna Story graduated in Chemical and Process Engineering from West Pomeranian University of Technology, Szczecin in 2012. She completed her PhD at the same University in 2017 in the area of non-Newtonian fluid flow in a stirred tank. She has been employed at the University since 2012 and, from 2017, has been an academic teacher. Her research interest is focused on rheology and non-Newtonian fluid flow in process equipment using experimental and numerical (CFD) techniques.

Grzegorz Story
Faculty of Chemical Technology and Engineering, West Pomeranian University of Technology, Aleja Piastow 42, 71-065, Szczecin, Poland
Grzegorz.Story@zut.edu.pl

Grzegorz Story graduated in Chemical and Process Engineering from West Pomeranian University of Technology, Szczecin in 2012. His PhD at the same University in 2017 was on dissolution of solid body in the magnetic field. He has worked for the university since 2016, since 2017 as a teacher. His research interest is focused on fluid flows in mixing tanks and the rotating magnetic field effect on transfer processes.